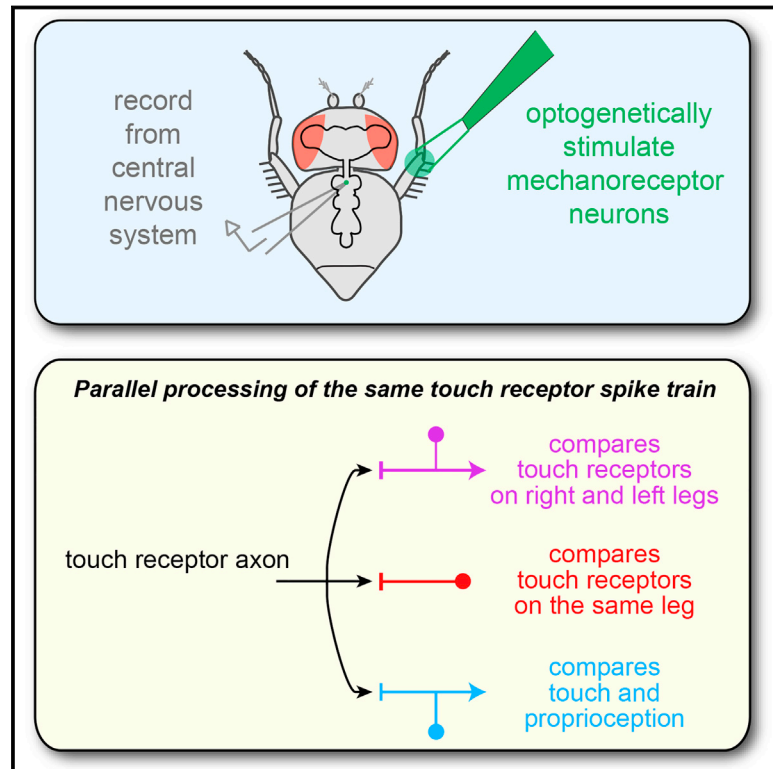


# Parallel Transformation of Tactile Signals in Central Circuits of *Drosophila*

## Graphical Abstract



## Authors

John C. Tuthill, Rachel I. Wilson

## Correspondence

rachel\_wilson@hms.harvard.edu

## In Brief

In vivo electrophysiology and 2-photon calcium imaging reveal that touch signals in *Drosophila* are sent in parallel to multiple genetically defined neuronal classes in the ventral nerve cord, which integrate excitatory and inhibitory inputs from other touch receptors and proprioceptors to encode unique stimulus features.

## Highlights

- Leg touch receptors project to at least three genetically defined neuron classes
- Each class integrates excitation and inhibition to compute a comparison
- Comparisons occur within a leg, across legs, and between touch and proprioception
- Each of these parallel neural circuits encodes a unique stimulus feature



# Parallel Transformation of Tactile Signals in Central Circuits of *Drosophila*

John C. Tuthill<sup>1,2</sup> and Rachel I. Wilson<sup>1,\*</sup>

<sup>1</sup>Department of Neurobiology, Harvard Medical School, 220 Longwood Avenue, Boston, MA 02115, USA

<sup>2</sup>Present address: Department of Physiology and Biophysics, University of Washington, 1705 NE Pacific Street, Seattle, WA 98195, USA

\*Correspondence: [rachel\\_wilson@hms.harvard.edu](mailto:rachel_wilson@hms.harvard.edu)

<http://dx.doi.org/10.1016/j.cell.2016.01.014>

## SUMMARY

To distinguish between complex somatosensory stimuli, central circuits must combine signals from multiple peripheral mechanoreceptor types, as well as mechanoreceptors at different sites in the body. Here, we investigate the first stages of somatosensory integration in *Drosophila* using *in vivo* recordings from genetically labeled central neurons in combination with mechanical and optogenetic stimulation of specific mechanoreceptor types. We identify three classes of central neurons that process touch: one compares touch signals on different parts of the same limb, one compares touch signals on right and left limbs, and the third compares touch and proprioceptive signals. Each class encodes distinct features of somatosensory stimuli. The axon of an individual touch receptor neuron can diverge to synapse onto all three classes, meaning that these computations occur in parallel, not hierarchically. Representing a stimulus as a set of parallel comparisons is a fast and efficient way to deliver somatosensory signals to motor circuits.

## INTRODUCTION

A tactile stimulus may recruit multiple mechanoreceptor types that encode different stimulus features (e.g., vibration versus pressure). Moreover, a stimulus may recruit neurons that encode the same stimulus feature at different locations on the body (e.g., vibration at two fingertips). Thus, downstream circuits must often integrate signals from multiple mechanoreceptor neurons in order to elicit appropriate behavioral responses. It is therefore fundamental to understand how signals from different mechanoreceptors are integrated in the CNS.

An important constraint on somatosensory integration is processing speed. Fast mechanosensory reflexes are an integral part of many motor behaviors (Burrows, 1996; Lundberg, 1979). For example, an insect can react to a mechanical stimulus within 20–30 ms (Jindrich and Full, 2002; Schaefer et al., 1994). A large fraction of this latency is due to mechanosensory transduction and axonal conduction (6–8 ms) (Höltje and Hustert, 2003; Ridgel et al., 2001), as well as the kinetics of muscle force production (10 ms) (Ahn et al., 2006). Thus, the central circuits that transform

sensory signals into motor commands are subject to tight constraints on speed.

In vertebrates, somatosensory integration may begin within a few synapses from the periphery. Indeed, some spinal cord projection neurons show evidence of both spatial pooling and cross-talk between different mechanoreceptor types (Brown and Franz, 1969; Wall, 1967). However, it has been difficult to identify the specific sites and mechanisms of somatosensory processing in vertebrates, partly due to the complications involved in recording from the spinal cord.

Here, we investigate the early stages of somatosensory processing in the fruit fly, *Drosophila*, which allowed us to combine *in vivo* single-cell electrophysiological recordings with genetic tools for labeling and manipulating specific neurons. A fly's sense of touch is mediated mainly by bristles that cover its body surface. Touching a bristle can evoke postural adjustment and grooming (Corfas and Dudai, 1989; Seeds et al., 2014; Vandervorst and Ghysen, 1980). Bristles may also contribute to tactile exploration (Pick and Strauss, 2005) and social interaction (Ramdya et al., 2015). However, nothing is known about how signals from bristle neurons are processed in the adult fly.

In this study, we show how signals from bristle neurons on the *Drosophila* leg are integrated and transformed in second-order somatosensory neurons of the ventral nerve cord (VNC), a region analogous to the vertebrate spinal cord. We identified three classes of second-order neurons that receive direct input from bristle touch receptors. One class compares touch signals from different locations on the same limb, whereas another performs bilateral comparisons across limbs, and another compares touch and proprioceptive signals. Notably, these different computations operate in parallel: we find that a single touch receptor axon can diverge to synapse onto all three cell classes. This parallel processing scheme may reflect an adaptation for speed.

## RESULTS

### Genetic Driver Lines for Leg Mechanoreceptor Neurons

Adult *Drosophila* possess four basic types of peripheral mechanoreceptor organs: bristles, hair plates, campaniform sensilla, and chordotonal organs (Figure 1A). Bristle neurons are the main touch receptors, and in this study, we focus on these neurons and their downstream targets. The other three organs are thought to serve mainly proprioceptive functions, based on studies in other insects (Burrows, 1996; Zill et al., 2004).

The axons of leg bristle neurons form a topographic map within the most ventral layer of the VNC neuropil. These axons

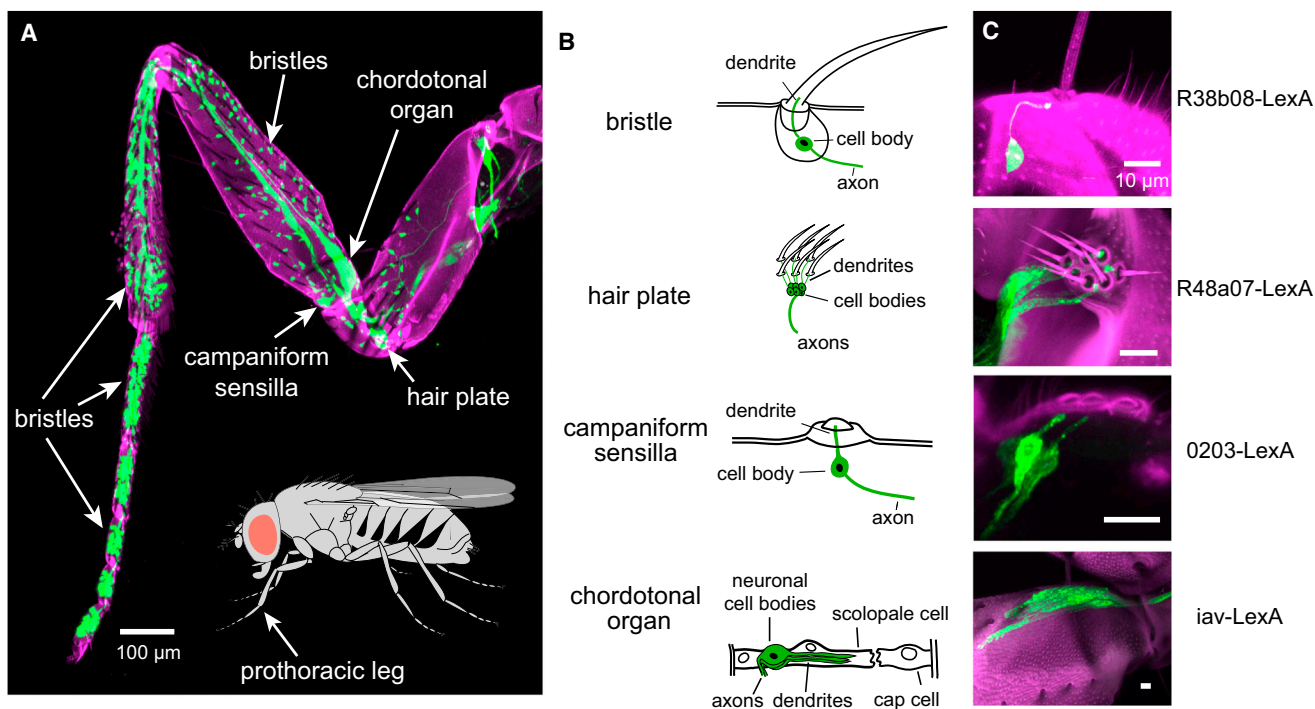


**Figure 1. Genetic Tools for Targeting Mechanoreceptor Neurons of the *Drosophila* Leg**

(A) Projection of a confocal stack through the prothoracic leg. GFP (green) is expressed in sensory neurons (under the control of *ChAT-Gal4*). Magenta shows cuticle autofluorescence.

(B) Schematic diagrams of each mechanoreceptor type. Associated mechanoreceptor neurons are in green.

(C) Projections of confocal stacks showing sensory neurons within each mechanoreceptor type. GFP (green) is expressed under the control of LexA. Magenta shows cuticle autofluorescence. Scale bars, 10  $\mu$ m.

See also [Figures S1](#) and [S2](#). See the [Supplemental Experimental Procedures](#) for all genotypes.

are largely segregated from the axons of other mechanoreceptor types, which project to more dorsal regions of the neuropil ([Meritt and Murphey, 1992](#); [Murphey et al., 1989a, 1989b](#); [Smith and Shepherd, 1996](#)). We took advantage of these distinct axonal arborization patterns to visually screen existing genetic libraries ([Gohl et al., 2011](#); [Jenett et al., 2012](#)) for LexA driver lines that labeled each mechanoreceptor type. We then further refined this screen by imaging GFP expression in the front (prothoracic) leg. In this way, we identified four LexA lines that delineate the four major mechanoreceptor types on the leg ([Figure 1](#); see [Figures S1](#), [S2](#), and [Supplemental Experimental Procedures](#) for details on each line). This LexA toolkit provides independent genetic access to neurons within each of the basic peripheral mechanoreceptor types.

### Propagation of Touch Signals in the Fly Ventral Nerve Cord

A single neuron resides at the base of each bristle. Mechanical stimulation of the bristle can evoke intense spiking activity within the bristle neuron ([Figure 2A](#)). Spiking activity in bristle neurons can also be driven optogenetically, by expressing the ChR2 variant Chrimson ([Klapoetke et al., 2014](#)) under the control of our LexA line specific for bristle neurons (*R38b08-LexA*), and illuminating the leg with green light ([Figure 2A](#)). These signals are recorded by clipping the bristle hair and placing a recording

electrode over the tip so that it makes electrical contact with the hair shaft; mounting the electrode on a piezoelectric actuator allows us to deliver calibrated mechanical stimuli to the bristle by moving the electrode itself ([Corfas and Dudai, 1990](#)).

To assess the number and location of central neurons that respond to bristle stimulation, we expressed the genetically encoded calcium indicator GCaMP6f ([Chen et al., 2013](#)) pan-neuronally, and we imaged the VNC with a 2-photon microscope ([Figure 2B](#)). Meanwhile, we optogenetically stimulated bristle neurons at the femur-tibia joint of the fly's left prothoracic leg ([Figure 2C](#)). We found that many VNC neurons displayed responses that were correlated with bristle neuron stimulation ([Figure 2D](#)). Specifically, in one representative fly, 69 of the 699 identifiable neuronal somata in the anterior portion of the VNC showed calcium bursts that were significantly correlated with stimulus pulses ([Figures 2E](#) and [2F](#)). We interpret this number as a lower bound on the number of responsive VNC neurons, due to the limited sensitivity of calcium imaging.

The VNC contains motor neurons in addition to the circuits that process sensory information. Motor neuron cell bodies are identifiable by their distinctively large size and characteristic position ([Baek and Mann, 2009](#); [Brierley et al., 2012](#)). We tentatively classified VNC neurons as either motor or non-motor based on their cell body size. Some putative motor neurons exhibited robust calcium signals correlated with bristle neuron stimulation

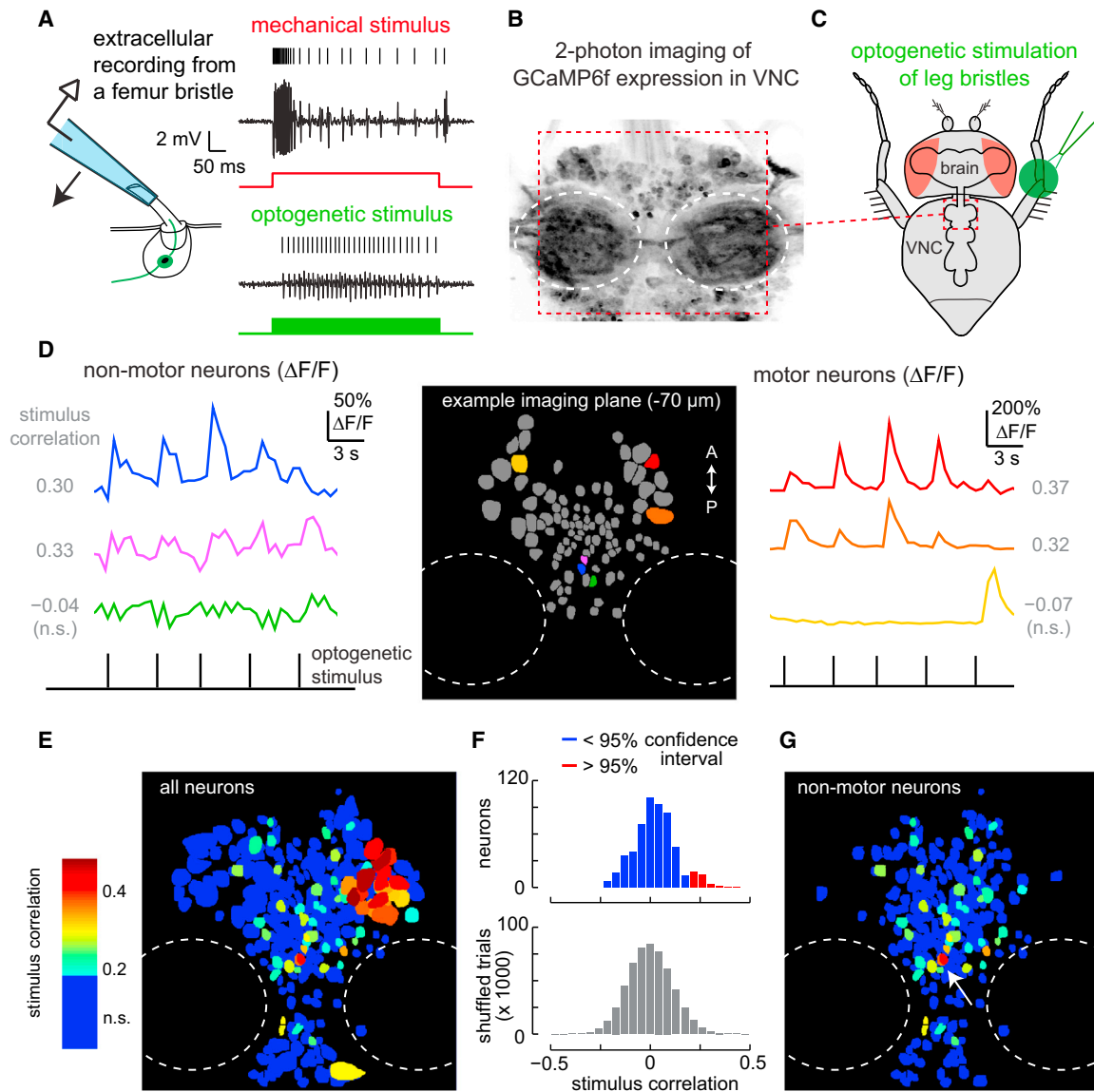


### Figure 2. Propagation of Touch Signals in the Fly Ventral Nerve Cord

(A) Left: schematic of bristle recording configuration. Right: responses of a bristle neuron to mechanical (red) and optogenetic (green) stimuli. Signals are band-pass filtered to facilitate spike identification (see [Supplemental Experimental Procedures](#)). All bristle neuron recordings are made from the same bristle on the prothoracic leg, near the femur-tibia joint ([Figure S5A](#)).

(B) Projection of a coronal stack through a region ( $\sim 180 \mu\text{m} \times 180 \mu\text{m}$ ) of the prothoracic ventral nerve cord (VNC) showing resting GCaMP6f fluorescence. GCaMP6f is expressed pan-neuronally and imaged with a two-photon microscope. Outlined in white dashed lines are the neuropil regions (neuromeres); these regions do not contain neuronal cell bodies.

(C) Schematic of optogenetic bristle stimulation for calcium imaging experiments. The fly is positioned ventral side up. Light is directed at the femur/tibia joint of a prothoracic leg. The imaged region of the VNC is outlined in red.

(D) GCaMP signals recorded during periodic optogenetic stimulation of leg bristles. The left and right panels show color-coded  $\Delta F/F$  responses of example neurons from a single imaging plane, illustrated in the center panel. Cross-correlation values, computed between each neuron's  $\Delta F/F$  signal and the stimulus waveform, are indicated alongside each trace.

(E) Map of all 699 neurons in the prothoracic region of a typical VNC, with individual neurons color-coded by their correlation value. In this projection, neurons with higher correlation are displayed on top. Neurons with correlation values below the threshold for statistical significance (0.19) are blue (n.s.).

(F) Top: distribution of correlation values between calcium signals ( $\Delta F/F$ ) and the stimulus waveform for all 699 neurons. Bottom: correlation values after shuffling the stimulus waveform; the 95<sup>th</sup> percentile of this distribution was taken as the threshold for significance.

(G) Correlation map of VNC neurons (same as E) but excluding motor neurons. The arrow points to the cluster of neurons that we identified for further scrutiny.

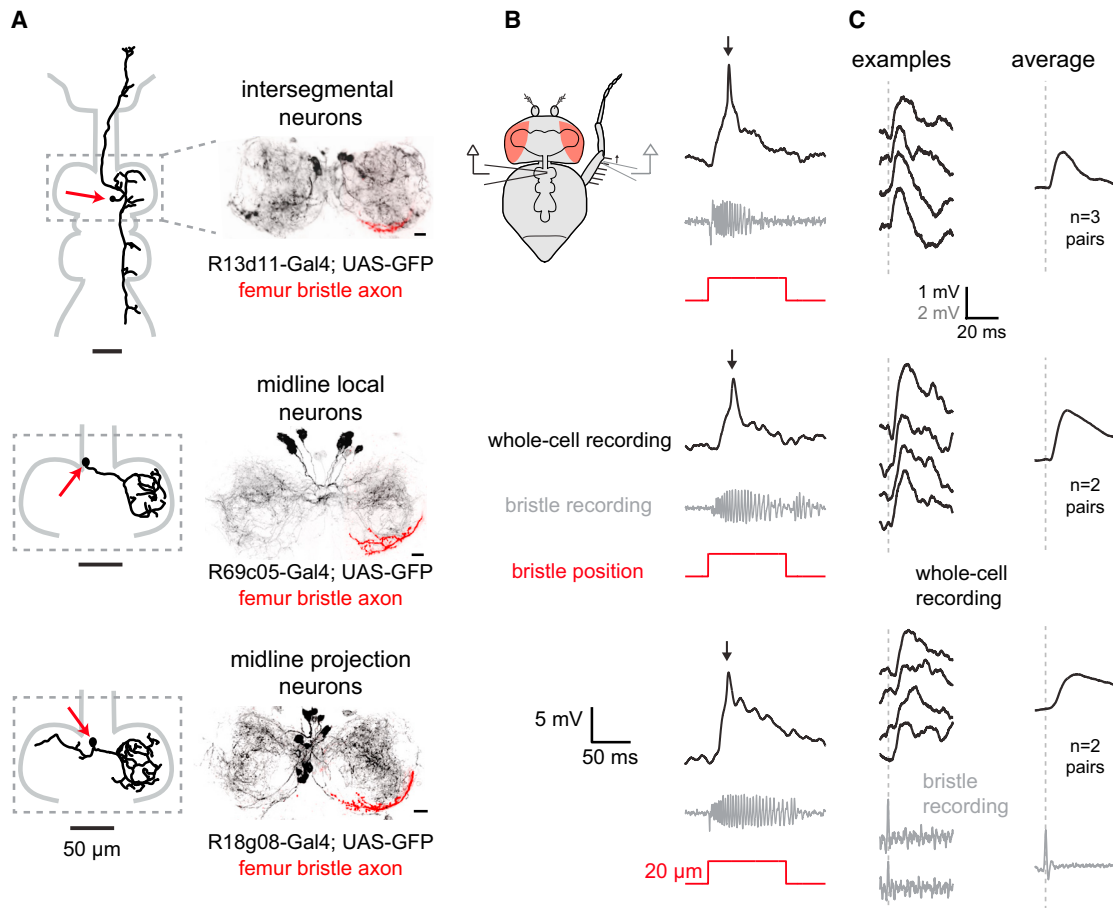


**Figure 3. Three Classes of VNC Neurons that Receive Direct Synaptic Input from the Same Femur Bristle**

(A) Left: morphology of a biocytin-filled neuron that expressed GFP in the indicated genotype. Red arrows indicate cell body position. Right: maximum intensity projection of GFP expression within the prothoracic neuromere of the VNC (black), co-labeled with the axonal arbor of a single femur bristle neuron filled with Dil (red); we always targeted the same femur bristle (Figure S5A). All three central neuron classes overlap with this bristle neuron axon. Scale bars, 10  $\mu$ m.

(B) Each row shows a typical *in vivo* whole-cell current-clamp recording from a central neuron and the simultaneously recorded signal from a bristle neuron. As before, we targeted the same bristle on the femur, near the femur-tibia joint (Figure S5A).

(C) Single spikes in this bristle neuron reliably trigger excitatory postsynaptic potentials (EPSPs) in each class of central neuron. As before, we targeted the same bristle on the posterior femur, near the femur-tibia joint (Figure S5A). Examples of bristle neuron spikes are shown at bottom. The left column shows representative single-trial EPSPs recorded from each corresponding central neuron class. At right are spike-triggered-averages of the postsynaptic voltage, averaged across all paired recordings from the same central neuron class where a connection was detected.

See also Figures S3, S4, and S5.

(Figures 2D and 2E), which may be related to the initiation of motor reflexes (Harris et al., 2015; Vandervorst and Ghysen, 1980). Because we were primarily interested in sensory processing, we excluded these putative motor neurons from our analysis. Of the remaining 43 neurons whose responses were significantly correlated with the stimulus, most were localized in a ventral cluster along the midline (Figure 2G). Based on these results, we focused our efforts on obtaining genetic access to neurons in this cluster.

### Three Cell Classes that Receive Direct and Divergent Synaptic Input from the Same Bristle Axon

To identify neurons postsynaptic to leg bristle neurons, we conducted another visual screen of genetic driver lines, this time focusing on the CNS. Because bristle neuron axons terminate

in the ventral layer of the VNC neuropil (Murphey et al., 1989b), we looked for neurons having dendrites in this zone. Guided by our calcium imaging results, we focused on neurons with somata in the ventral cluster along the midline. Candidate lines that emerged from this visual screen were then re-screened electrophysiologically: we labeled neurons with GFP, and we made visually targeted *in vivo* whole-cell recordings from neuronal somata while deflecting bristles at the femur-tibia joint of the fly's left prothoracic leg.

We identified three neuron classes that reliably responded to this mechanical stimulus (Figures 3 and S3), each labeled by a distinct Gal4 line. The first of these lines (*R13d11-Gal4*) labeled intersegmental neurons with axons that ascended through the neck connective to the brain. The second line (*R69c05-Gal4*) labeled midline local neurons that arborized within a single

segment (neuromere) of the VNC. The third line (*R18g08-Gal4*) labeled midline projection neurons that arborized mainly in the ipsilateral neuromere, but also sent a projection to the contralateral neuromere. Within each neuron class, all recorded cells exhibited consistent morphological and intrinsic electrophysiological properties. Antibody staining against candidate neurotransmitters indicated that the midline local neurons and midline projection neurons are likely glutamatergic, while at least some of the intersegmental neurons are likely cholinergic (Figure S4).

In total, the three neuron classes we identified contained ~14 cells on the left side of the prothoracic VNC and the same number on the right. Recall that, in a typical fly, 43 putative non-motor neurons showed significant calcium responses to stimulating bristle neurons on the fly's left prothoracic leg near the femur/tibia joint. The cell classes we have identified represent a sizeable fraction of that number (14/43). Thus, these neurons likely represent a substantial component of the VNC neurons that respond to touch on this region of the leg.

All three classes of VNC neurons are anatomically positioned to receive direct synaptic input from bristle neurons. Evidence for this came from filling an identified femur bristle neuron (indicated in Figure S5A) with a fluorescent dye. The dendrites of all three central neuron classes roughly overlapped with the bristle neuron axon terminal, indicating the potential for direct connectivity (Figures 3A and S5B).

We confirmed that some neurons within each class are postsynaptic to this same femur bristle neuron by making paired electrophysiological recordings from the bristle neuron and individual central neurons. Movement of this bristle elicited a train of spikes in the bristle neuron and it evoked a large depolarization and a single spike in most of the central neurons we recorded from. This was true of all intersegmental neurons (eight of eight), most midline local neurons (six of seven), and most midline projection neurons (five of eight) (Figure 3B). All central neuron responses to bristle stimulation were completely blocked by bath application of the nicotinic acetylcholine receptor antagonist methyllycaconitine (MLA, 1  $\mu$ M; data not shown), indicating that bristle neurons release acetylcholine.

In a subset of the recordings where we found a connection between a bristle neuron and a central neuron, we were able to evoke single spikes in the presynaptic bristle neuron by making a very small movement of the bristle (<5  $\mu$ m). In every one of these cases, and for all cell classes, we found that a single bristle spike produced a reliable excitatory postsynaptic potential (EPSP) in the central neuron (Figure 3C). The trial-averaged latency of these responses was similar across all three cell classes (~3 ms; Figure S6A). The trial-to-trial SD in the latency of these responses was relatively small (typically <1 ms). Because a single presynaptic spike is sufficient to elicit an EPSP, and because the EPSP has a consistent latency of about 3 ms, we can conclude that this is a monosynaptic connection.

Together, these results indicate that some neurons within all three classes are directly postsynaptic to bristle neurons. Moreover, because all these experiments targeted one specific femur bristle, we can conclude that some neurons within all three classes receive input from a common bristle afferent.

### Intersegmental Neurons Compare Touch and Proprioceptive Inputs

We next turned our attention to the central integration of touch signals, considering each central neuron class in turn. We began with the intersegmental neurons. *R13d11-Gal4* labels two pairs of intersegmental neurons in each prothoracic neuromere, each of which extends an anterior process that ascends to the brain, and a posterior process that innervates the meso- and metathoracic neuromeres (Figure 4A). Biocytin fills revealed that, within each pair, one intersegmental neuron projects to the ipsilateral side of the brain, the other to the contralateral side, where they both arborize in a brain region called the vest (Figures S3B and S5C). The dendrites of every intersegmental neuron branch throughout the ventral prothoracic neuromere, in the same region where leg bristle axons terminate.

We mapped the touch receptive fields of intersegmental neurons using both mechanical and optogenetic stimulation of leg bristles. For mechanical stimulation, we used a probe mounted on a piezoelectric actuator to deflect one or two bristles, taking care not to touch the cuticle to avoid stimulating proprioceptors. For optogenetic stimulation, we expressed Chrimson in bristle neurons and illuminated small regions of the leg (~200  $\mu$ m in diameter). Mechanical stimuli allowed us to investigate how central neurons respond to activation of one or two bristle neurons, while optogenetic stimuli revealed how downstream neurons respond to activation of many bristle neurons.

We found that intersegmental neurons receive excitatory synaptic input from bristles along the entire length of the leg (Figures 4A and 4B). Mechanical and optogenetic mapping methods always produced similar results. Optogenetic stimulation of the distal leg produced somewhat larger responses than did stimulation of the proximal leg; this is likely because bristles are most heavily concentrated on the distal leg (Figure 1A).

Touch receptors may be activated during self-movement—for example, when the leg touches an obstacle during walking. Comparing activity in touch receptors and proprioceptors might allow downstream neurons to contextualize touch signals during self-generated movement. Therefore, we investigated whether these central neurons integrate signals from leg proprioceptors. In separate experiments, we drove expression of Chrimson in each of the three major proprioceptor types (Figure 1) and optogenetically stimulated mechanoreceptors on the leg while recording from GFP-labeled intersegmental neurons in the VNC. We discovered that optogenetic stimulation of leg chordotonal neurons hyperpolarized the intersegmental neurons (Figures 4C–4E). This effect was specific to chordotonal neurons, because we found no response to stimulation of the other two proprioceptor types, hair plate neurons or campaniform sensilla (Table S1).

To assess the functional consequences of proprioceptive inhibition, we combined optogenetic activation of chordotonal neurons with mechanical stimulation of bristles on the tibia. Inhibition driven by chordotonal neurons reduced touch-evoked excitation, as measured by either peak membrane depolarization or spike rate (Figures 4D and 4E). Thus, proprioceptive inhibition from chordotonal neurons can suppress excitatory touch signals in these central neurons.

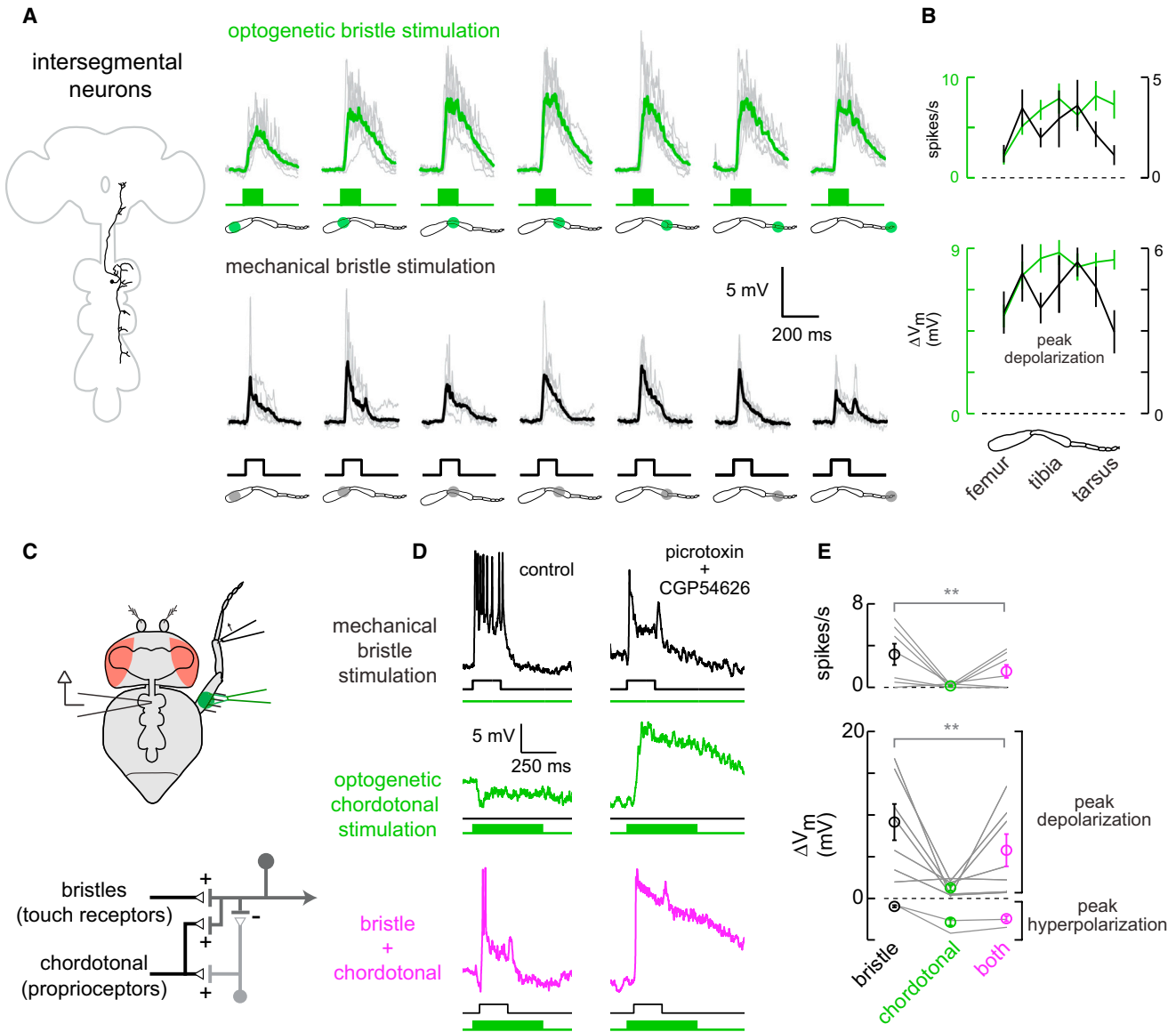


**Figure 4. Intersegmental Neurons Compare Touch and Proprioceptive Inputs**

(A) Top: membrane potential responses of intersegmental neurons to optogenetic stimulation of bristle neurons (individual cells in gray, average in green,  $n = 9$ ). Bottom: responses of a subset of the same neurons to mechanical stimulation of small numbers of bristles (individual cells in gray, average in black,  $n = 6$ ).

(B) Average spike rates and peak voltage changes for the cells shown in (A), mean  $\pm$  SEM across cells, plotted versus stimulus location. Optogenetic responses are in green, mechanical responses in black.

(C) Top: bristle neurons on the distal tibia are stimulated mechanically, and the femoral chordotonal organ is stimulated optogenetically. Bottom: proposed circuit diagram for sensory inputs converging onto intersegmental neurons, with proprioceptive inhibition routed via an interposed inhibitory interneuron. Chordotonal neurons also drive excitation (directly or indirectly), but this is normally masked by inhibition.

(D) Inhibitory input driven by chordotonal neurons suppresses excitatory input from leg bristle neurons. The top and middle rows show responses of a typical intersegmental neuron to stimulation of bristle neurons or chordotonal neurons alone. In the bottom row, the two stimuli are delivered together. The optogenetic stimulus precedes the mechanical stimulus and is more prolonged, in order to increase the effect of inhibition. Antagonists of synaptic inhibition (100  $\mu$ M picrotoxin and 50  $\mu$ M CGP54626) block the suppressive effect of chordotonal neuron stimulation, revealing underlying excitation; similar effects were seen in a total of six experiments (data not shown). The postsynaptic neuron is not spiking in the presence of antagonists because the neuron has been depolarized to the point where it cannot initiate spikes.

(E) Average spike rates and peak voltage changes,  $\pm$  SEM across cells, for all experiments like that shown in the left column of (D). Inhibition driven by chordotonal neurons significantly suppressed responses to bristle neuron stimulation ( $n = 9$  cells,  $**p = 0.03$  for depolarization and  $p = 0.03$  for spikes, Wilcoxon signed rank test).

See also Figures S3, S4, S5, and S6 and Table S1.

Antagonists of inhibitory neurotransmitter receptors (100  $\mu$ M picrotoxin and 50  $\mu$ M CGP54626) blocked inhibition driven by chordotonal neurons and revealed underlying excitation from chordotonal neurons (Figure 4D). Inhibition driven by chordotonal neurons was also blocked by an antagonist of nicotinic receptors (MLA, 1  $\mu$ M;  $n = 2$ , data not shown), as we would expect if chordotonal neurons were cholinergic and excited inhibitory interneurons via nicotinic synapses.

These data are most consistent with a circuit model in which intersegmental neurons receive indirect inhibitory input from chordotonal neurons via interposed inhibitory interneurons (Figure 4C). Excitation from chordotonal neurons (which may be direct or indirect) is normally masked by this inhibitory input.

Overall, these data demonstrate that the touch processing system integrates signals from distinct mechanoreceptor types at the first stage of central circuitry—i.e., in neurons directly postsynaptic to peripheral afferents. This cross-modal comparison could allow intersegmental neurons to encode specific conjunctions of touch and proprioceptor signals.

#### Midline Local Neurons Compare Proximal and Distal Touch within a Leg

In contrast to the long-range projections of the intersegmental neurons, the arbors of midline local neurons are limited to a single neuromere. *R69c05-Gal4* labels 12–16 midline local neurons within the prothoracic region of the VNC, and each neuron exclusively innervates either the left or right neuromere (Figure 5A). Every neuron we filled within this class had a similar morphology. Their processes were restricted to the ventral edge of the neuropil, in the same region where leg bristle axons terminate (Figure S3).

The spatial receptive fields of midline local neurons were more sharply tuned than those of the intersegmental neurons. Only the distal leg produced strong excitation. The proximal leg produced weak excitation if the stimulus was mechanical, and weak excitation followed by inhibition if the stimulus was optogenetic (Figures 5A and 5B). The difference between optogenetic and mechanical stimulation likely reflects the fact that the optogenetic stimulus recruits dozens of bristle neurons, whereas the mechanical stimulus recruits only one or two. The difference in the postsynaptic response suggests a nonlinearity in the recruitment of inhibition: stimulation of a few bristles on the proximal leg is not sufficient to recruit inhibition, but co-stimulation of many bristles produces a net inhibitory effect, suggesting that a threshold for recruiting inhibition has been crossed. Midline local neurons did not respond to input from chordotonal neurons, campaniform sensilla, or hair plates (Table S1). Thus, unlike the intersegmental neurons, they specifically receive input from a single mechanoreceptor type.

We investigated the integration of excitatory and inhibitory touch signals through combined activation of proximal and distal bristles (Figures 5C–5E). We found that optogenetic stimulation of proximal (femur) bristles produced inhibition that suppressed excitatory responses to mechanical stimulation of distal (tibia) bristles (Figures 5D and 5E). Picrotoxin abolished this inhibition and unmasked an excitatory response to femur bristle stimulation (Figure 5D). All postsynaptic responses were eliminated by

blocking nicotinic receptors with 1  $\mu$ M MLA ( $n = 3$  cells, data not shown).

These data suggest that inhibition to midline local neurons is supplied by inhibitory interneurons that receive excitatory input from femur bristles (Figure 5C). The nonlinearity in the recruitment of inhibition might reside, for example, in the spike threshold of this interneuron. Excitation from femur bristles is normally masked by inhibition. The dominant excitatory input to the midline local neurons is from the bristle neurons of the distal leg.

Thus, in contrast to the intersegmental neurons—that compare touch and proprioceptive inputs—we find that the midline local neurons compare touch inputs from the proximal and distal regions of the leg. This local computation should allow the midline local neurons to respond preferentially to objects that touch the distal leg, regardless of the size of the object or the magnitude of the force it exerts. It may not be a coincidence that the distal leg has the highest density of bristles and it is most likely to contact objects during walking and tactile exploration.

#### Midline Projection Neurons Compare Touch Stimuli across Contralateral Legs

The final cell class we studied consisted of the midline projection neurons. *R18g08-Gal4* labels a group of 10–14 neurons with a distinctive bilateral morphology. Each neuron arborizes in both the left and right neuromeres, and one arborization is larger than the other (Figures 6A and S3). The cell body is typically located contralateral to its principal arbor.

These neurons responded exclusively to bristle stimulation. They were unresponsive to stimulation of chordotonal neurons, campaniform sensilla, or hair plates (Table S1). Thus, like the midline local neurons, and unlike the intersegmental neurons, they specifically receive input from a single mechanoreceptor type.

As suggested by their morphology, we discovered that each of the midline projection neurons integrates touch input from both legs. We first used optogenetic stimuli to map bristle inputs from both the ipsilateral and contralateral legs (relative to the principal arbor). Each neuron was dye-filled and anatomically reconstructed to verify its orientation. Every recorded neuron had a similar morphology.

In general, we found that optogenetic stimulation of bristle neurons evoked a mix of excitation and inhibition (Figure 6A). Ipsilateral inputs were typically stronger and more likely to be excitatory, although we found a few ipsilateral inhibitory responses as well. By comparison, contralateral inputs were weaker and more often inhibitory. As a group, the midline projection neurons had relatively diverse receptive field structures, although all were bilateral, and most combined excitation and inhibition. The most common pattern was ipsilateral excitation and contralateral inhibition. Other cells received net excitation from both the ipsilateral and contralateral legs. Mechanical stimulation of one or two bristles produced exclusively excitatory responses, which were largest for distal leg regions (Figure S7A). Again, we attribute differences between optogenetic and mechanical receptive fields to the fact that optogenetic stimuli drive activity in dozens of bristle neurons, whereas our mechanical

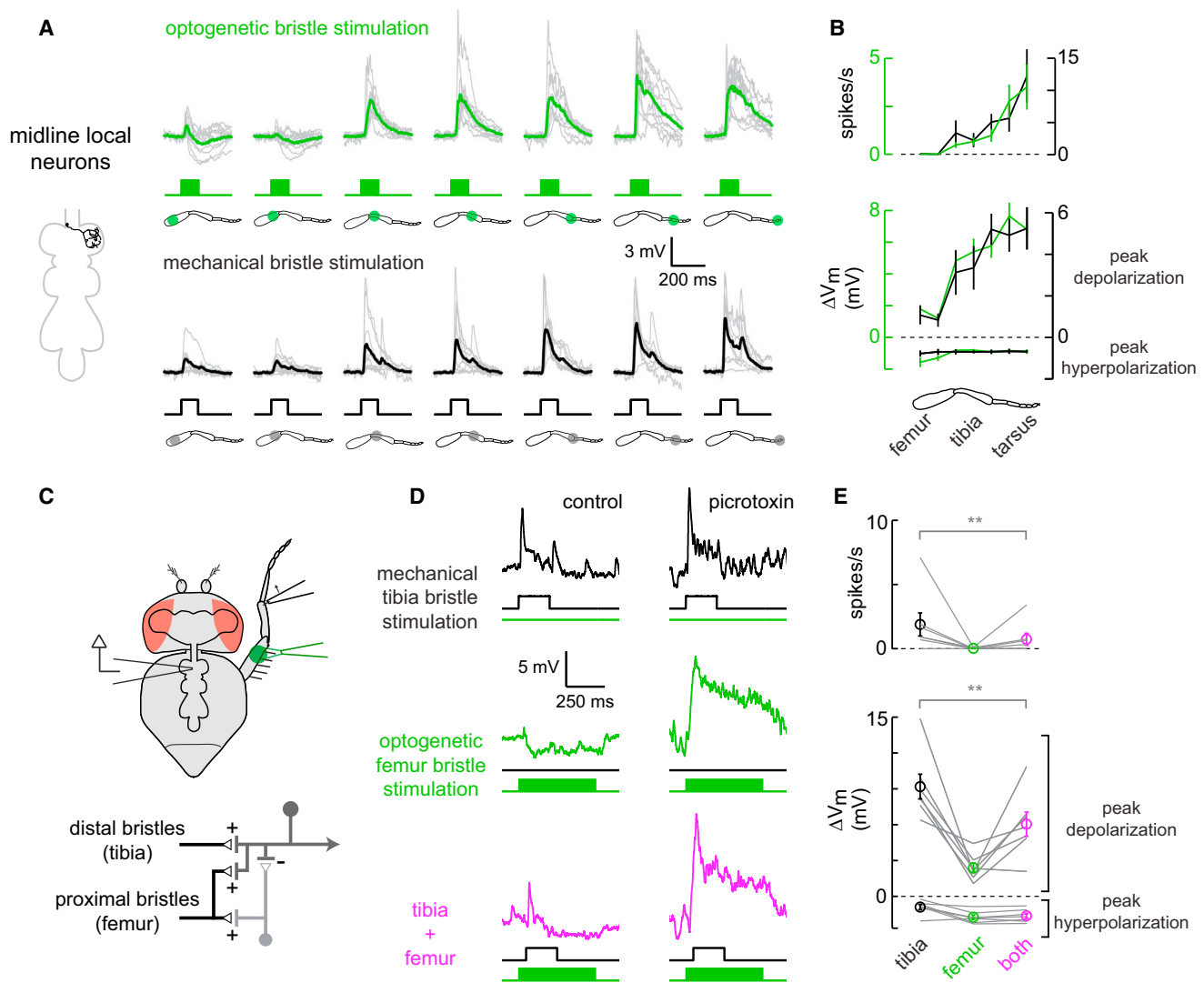


**Figure 5. Midline Local Neurons Compare Proximal and Distal Touch within a Leg**

(A) Responses of midline local neurons, as in Figure 4 ( $n = 10$  for optogenetic stimuli,  $n = 9$  for mechanical stimuli).

(B) Average spike rates and peak voltage changes for the cells shown in (A), mean  $\pm$  SEM across cells.

(C) Top: to elicit combined distal and proximal touch inputs, bristle neurons on the distal tibia are stimulated mechanically, and bristle neurons on the femur are stimulated optogenetically. Bottom: proposed circuit diagram for sensory inputs converging onto local neurons, with proximal inhibition routed via an interposed inhibitory interneuron.

(D) Inhibitory input driven by proximal femur bristle neurons suppresses excitatory input from distal tibia bristle neurons. Top and middle: responses of a midline local neuron to stimulation of femur or tibia bristle neurons alone. Bottom: the two stimuli are delivered together. Picrotoxin ( $10 \mu\text{M}$ ) blocks the suppressive effects of femur bristle stimulation, revealing underlying excitation; similar effects were seen in a total of four experiments.

(E) Average spike rates and peak voltage changes,  $\pm$  SEM across cells, for all experiments like those shown in the left column of (D). Inhibition from femur bristles significantly suppressed excitatory signals from tibia bristles ( $n = 7$  cells,  $**p = 0.02$  for depolarization and  $p = 0.03$  for spikes, Wilcoxon signed rank test).

See also Figures S3, S4, and S6 and Table S1.

stimuli are confined to one or two bristles. As inhibition is only recruited by optogenetic stimulation, it likely requires co-activation of many bristle neurons.

To examine bilateral integration of touch signals in these neurons, we optogenetically stimulated bristle neurons on the tibia of the right and left prothoracic legs (Figure 6B). Two example experiments of this type are shown in Figure 6C. In the first example, inhibition from the contralateral leg reduced

excitation from the ipsilateral leg. In essence, a neuron like this is comparing input to the right and left legs. This should allow such a neuron to respond preferentially to an object touching the ipsilateral leg only. In the second example, ipsi- and contralateral excitation combined additively. This neuron should respond best to an object that is touching both legs. Across the population, combining ipsilateral and contralateral stimulation evoked a variety of results (Figure S7C). In all cases, picrotoxin eliminated

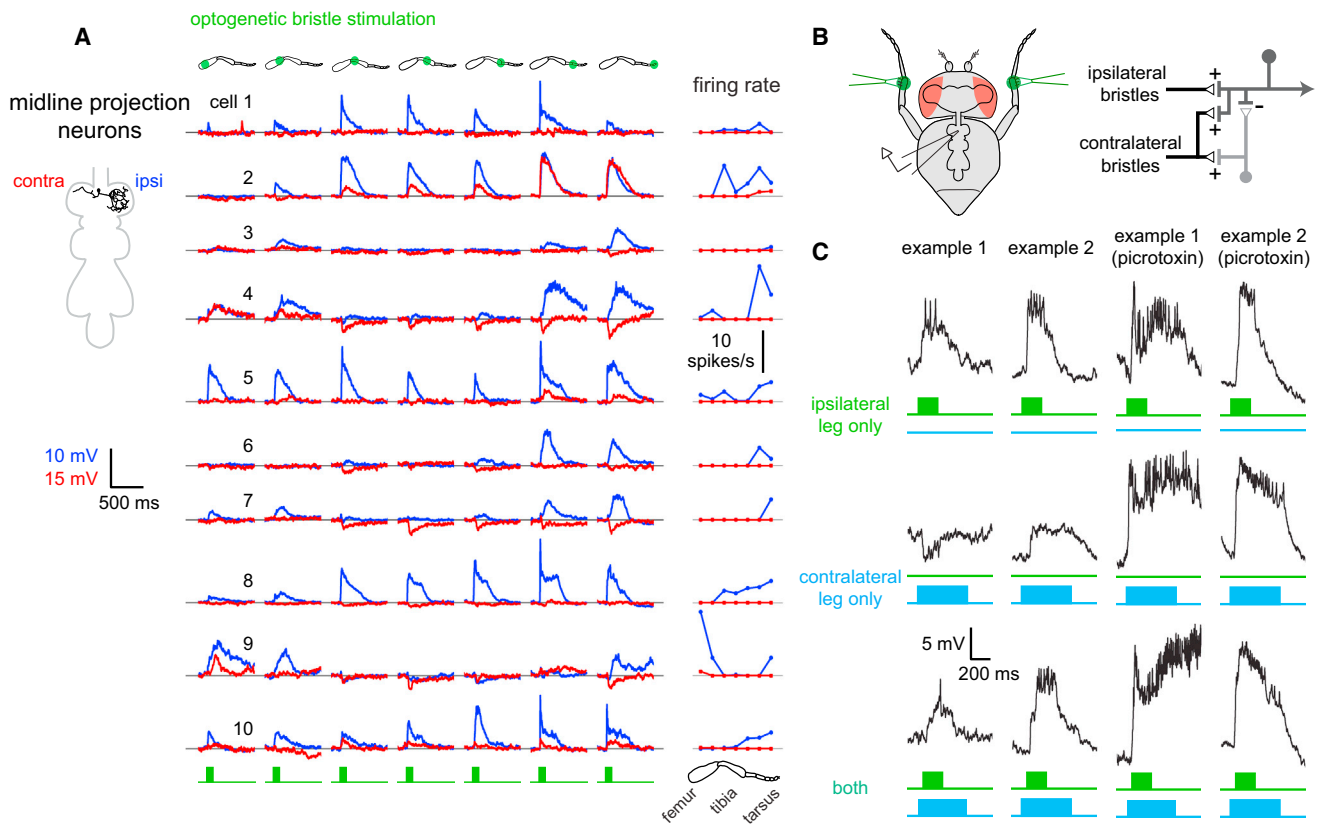


**Figure 6. Midline Projection Neurons Compare Touch Stimuli across the Body Midline**

(A) Trial-averaged responses of ten midline projection neurons to optogenetic stimulation of bristle neurons. For each neuron, responses were measured for both the ipsilateral (blue) and contralateral (red) prothoracic legs. Ipsilateral is defined as the side containing the reconstructed neuron's primary arborization (schematic at left). The right column shows trial-averaged spike rates versus stimulus location.

(B) Left: schematic of the recording configuration. Bristles on the contralateral and ipsilateral tibia are stimulated optogenetically. Right: proposed circuit diagram for those midline projection neurons that combine ipsilateral excitation with contralateral inhibition.

(C) Integration of touch signals across legs. Top and middle: responses of local neurons to independent stimulation of ipsilateral and contralateral bristles. Bottom: the two stimuli are delivered together. Picrotoxin (10  $\mu$ M) blocks inhibition from contralateral bristles, revealing excitation (Figure S7B). Data for all experiments of this type are shown in Figure S7.

See also Figures S3, S4, and S6 and Table S1.

inhibition evoked by optogenetic bristle neuron stimulation (Figure 6C) and uncovered latent excitatory inputs along the entire length of both legs (Figure S7B). This result suggests that midline projection neurons receive broad excitatory input from leg bristles, which is suppressed by concomitant inhibition in some regions of the leg. Thus, as with the midline local neurons, excitation appears to be spatially broader than inhibition. Although these receptive fields were diverse, the most common pattern appears to be ipsilateral excitation combined with contralateral inhibition, with inhibition likely relayed through interposed inhibitory neurons (Figure 6B). As a population, these neurons may play a role in behaviors that involve right-left coordination based on touch cues, such as during walking, grooming, or courtship.

#### Parallel Somatosensory Pathways Encode Distinct Features of Complex Movements

Up to this point, we have shown that three classes of VNC neurons perform distinct computations on the same touch input.

However, all of these experiments used a very restricted range of mechanical stimuli. Normally, the fly would be able to stimulate leg bristles and proprioceptors through self-movement, and the mechanical forces impinging on the leg would be more complex. Given what we know about these cell classes, we would expect them to encode distinct but overlapping features of complex stimuli.

To explore this idea, we allowed the fly to freely move its legs while we performed simultaneous whole-cell recordings from pairs of VNC neurons. During these recordings, the prothoracic leg frequently collided with the other legs or with the recording platform, likely stimulating touch and proprioceptive mechanoreceptor neurons on the legs. Two representative recordings are shown in Figure 7. In these experiments, we first used the piezoelectric actuator to mechanically stimulate a femur bristle and confirm that both central neurons responded (Figures 7A and 7D), as expected from our previous results (Figure 3). After we confirmed responses to controlled

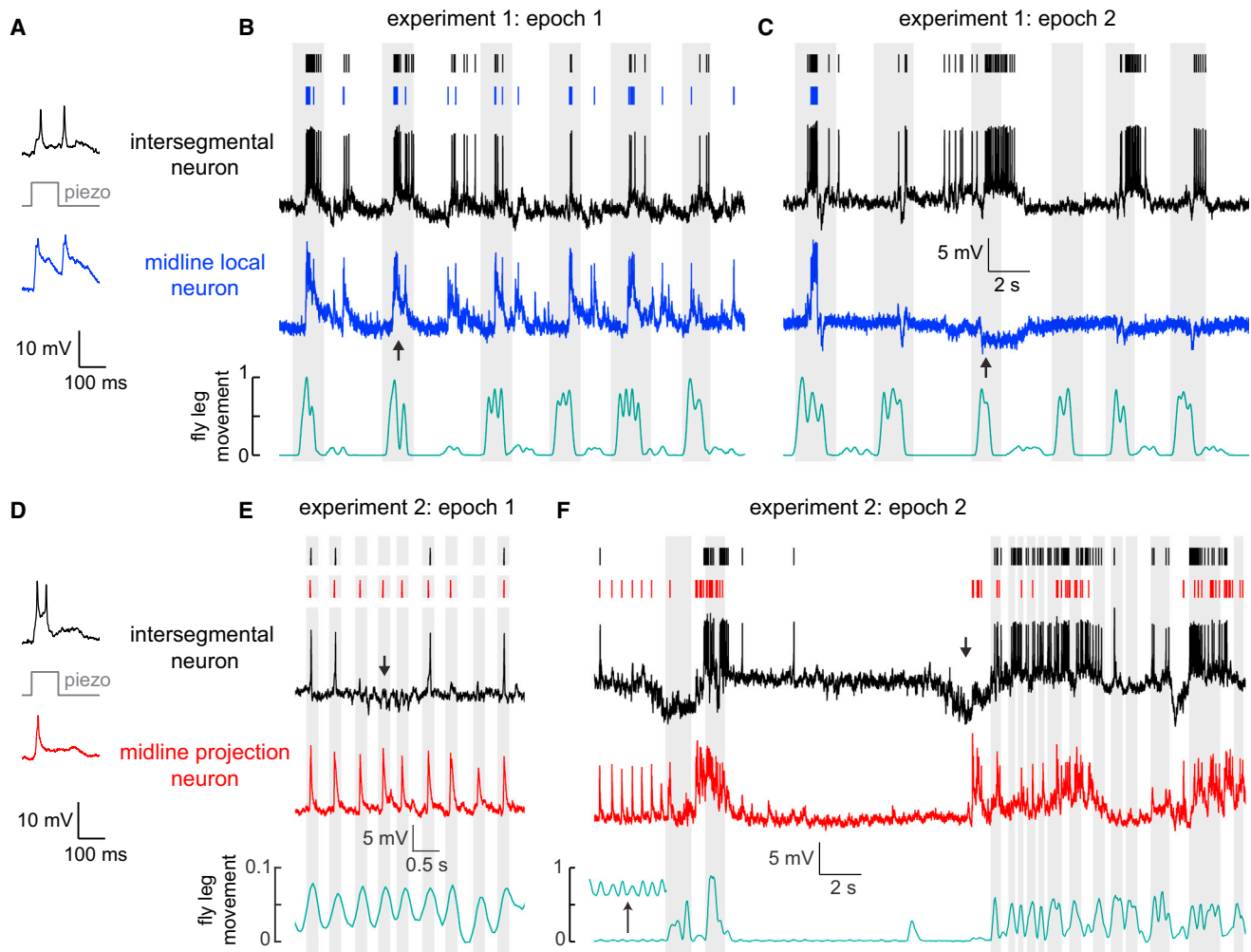


**Figure 7. Parallel Coding of Complex Stimuli in Simultaneously Recorded Central Neuron Pairs**

(A) Paired whole-cell recording from an intersegmental neuron and a midline local neuron. Example traces show the simultaneous responses of the two neurons to mechanical stimulation of a femur bristle. These responses confirm that this particular pair of neurons share input from some of the same bristles (Figure 3).

(B) During this epoch of the experiment, the fly makes large movements that cause both neurons to depolarize and fire correlated bursts of spikes (e.g., at the arrow). Fly movement is quantified in a.u. (see Supplemental Experimental Procedures). Movement bouts are shaded in gray. Spike times are represented with rasters above the raw voltage traces.

(C) During a later epoch of the same experiment, the midline local neuron stops being excited during movement bouts and is instead inhibited by movement (e.g., at the arrow). This change corresponds to a switch between large movements of multiple legs, to smaller movements of the prothoracic leg.

(D) Same as (A) but for a simultaneously recorded intersegmental and a midline projection neuron.

(E) The same pair of neurons as in (D), but now responding to spontaneous movement. Small periodic twitching movements of the fly's leg (gray shading) evoke reliable responses in the midline projection neuron, but not in the intersegmental neuron. The periodic responses of the intersegmental neuron are interrupted by barrages of inhibitory postsynaptic potentials (e.g., at the arrow). Note the expanded vertical scale of the movement measurements.

(F) During a later epoch of the same experiment, the fly spontaneously switches from twitching to making larger movements of the entire leg. The midline projection neuron is depolarized during large movement bouts, while the intersegmental neuron responds with sequences of inhibition and excitation at movement onset (e.g., at the arrow). The inset in the movement trace (bottom) shows periodic movement on a 10-fold expanded vertical scale.

mechanical stimuli, we provoked the fly with a flash of light, causing it to initiate complex movements. Epochs of large struggling movements alternated with epochs of low-amplitude squirming. During different epochs, the leg was in a different part of its movement range, and different parts of the leg were touched. As the fly transitioned between epochs, we observed changes in the patterns of correlation among different VNC neurons.

In the first experiment illustrated here, the fly initially made large movements of multiple legs. During this epoch, the responses of an intersegmental neuron and a midline local neuron were tightly correlated with each other and also correlated with leg movement (Figure 7B). Later, the fly switched to making smaller amplitude movements of the prothoracic leg. Now the activity of the two neurons became anti-correlated: movement produced excitation in the intersegmental neuron and inhibition

in the midline local neuron (Figure 7C). Recall that midline local neurons receive substantial inhibition driven by bristle neurons, while bristle neuron input to intersegmental neurons is mainly excitatory; this finding may explain why these neurons can be anti-correlated during certain epochs.

In the second experiment illustrated here, we also observed periods of correlated and anti-correlated activity (Figures 7D–7F). Here, the fly initially made small periodic twitching movements, during which midline projection neuron spiked on each movement cycle, while the simultaneously recorded intersegmental neuron showed more irregular activity and was occasionally hyperpolarized during movement (Figure 7E). Later, the fly switched to making large movements of the entire leg. Now the relationship between the two neurons changed: the midline projection neuron was depolarized during each movement bout, whereas the intersegmental neuron responded with an inhibition-excitation sequence (Figure 7F). Recall that the intersegmental neurons receive inhibition driven by proprioceptors (Figure 4), whereas the midline projection neurons do not receive proprioceptive input (Table S1). This finding may explain why these two cell classes can be anti-correlated during certain epochs.

These complex mechanical stimuli revealed relationships among VNC neurons that were not observed in previous experiments with simpler stimuli. Given these complex stimuli, we found that pairs of VNC neurons were positively correlated during some epochs, but uncorrelated or even anti-correlated during other epochs. This makes sense if each cell encodes a distinct feature of the mechanical forces acting on the body. When these features are temporally correlated, these fire together; when these features are anti-correlated, these cells become opponent to each other.

## DISCUSSION

In this study, we used somatosensory circuits in the *Drosophila* VNC to investigate the neural computations that occur at the first stages of touch processing. Our results suggest a conceptual framework for the central integration of peripheral touch signals. First, signals from peripheral touch receptors are directly transmitted to multiple, parallel processing channels. Within these channels, spatial selectivity is achieved through integration of excitatory and inhibitory inputs from touch receptors in different locations. In parallel, contextual selectivity is achieved by integrating touch signals with information from proprioceptors.

### Comparisons as the Building Blocks of Efficient Codes

One idea unites the three CNS cell classes we describe here. Namely, cells within all three classes are performing comparisons—within a limb, across limbs, or between different mechanoreceptor types (Figures 4, 5, and 6). These comparisons encode the difference between mechanical stimuli of different types, and/or mechanical stimuli at different sites on the body. In general terms, any neuron with an inhibitory receptive field component is encoding a comparison. What is notable in our results is the observation that different central neurons directly postsynaptic to the same afferent axon are performing a variety of different comparisons. At the very first synapse of the somatosensory system, excitation from a given afferent is being inte-

grated with inhibition from several different sources, with each type of comparison occurring in a distinct parallel processing channel. Collectively, these comparisons span a wide range of spatial scales, even though they are all being performed one synapse from the periphery.

Encoding sensory information via comparisons brings several advantages. When a neuron computes the difference between two input signals, the shared component of those input signals is suppressed. This arrangement can allow neurons to transmit finer spatial or temporal features of a stimulus (Srinivasan et al., 1982) and reduce redundancy among the spike trains of different neurons (Barlow, 1961), thereby increasing metabolic efficiency (Niven and Laughlin, 2008). This strategy may be particularly useful in a system facing an information bottleneck. In this case, the relevant bottleneck is the neck of the fly, which contains only ~3,600 axons (Hengstenberg, 1973). Among the cell classes we study here, one projects directly to the brain (the intersegmental neurons), while the others may relay information indirectly to the brain, as well as participating in local VNC reflex circuits.

### Parallel Processing as an Adaptation for Speed

Here, we show that an individual touch receptor axon diverges to directly contact multiple postsynaptic cell classes, each performing a different parallel computation. Why perform these computations in parallel, rather than hierarchically? One important consideration is the necessity for speed. Speed may be a particularly important constraint in somatosensory processing, because the site of sensory transduction (e.g., the foot) can be relatively distant from the CNS. Because *Drosophila* axons are unmyelinated and usually narrow, axonal conduction is likely to be slow. Indeed, we measured a consistent delay of about 3 ms from the time of a femur bristle neuron spike in the periphery to the onset of an EPSP in the VNC (Figure S6A). This delay is presumably even longer for mechanosensory signals arising from the distal leg, since the axons of tarsus bristle neurons can be over twice as long as the axons of femur bristle neurons.

### Bilateral Comparison across Limbs

Some of the central neurons we describe here—the midline projection neurons—integrate information from the right and left legs. Although we observed considerable receptive field diversity within this neural population, the general receptive field structure consisted of ipsilateral excitation, together with mixed excitation and inhibition from the contralateral leg (Figure 6). This organization is similar to that of some neurons in vertebrate spinal cord (Brown and Franz, 1969) and somatosensory cortex (Iwamura, 2000), which integrate excitatory input from one side of the body with mixed excitation and inhibition from the opposite side.

Bilateral tactile integration is clearly important to some behaviors. For example, rats can distinguish the relative distance of two walls using their whiskers, a behavior that requires activity in somatosensory cortices of both hemispheres (Shuler et al., 2002). In a similar manner, integrating touch signals from the two legs may allow the fly to compare bilateral tactile features. For example, when faced with a small gap, flies reach forward across the void with their front legs and attempt to cross only when both legs have contacted the opposite side (Pick and

Strauss, 2005). Comparison of bilateral somatosensory signals is also critical for the refinement of rhythmic motor behaviors, such as crawling in *Drosophila* larvae (Heckscher et al., 2015).

### Integration of Touch and Proprioception

In vertebrates, different types of peripheral mechanoreceptors have been traditionally considered to be functionally segregated pathways. Different mechanoreceptor types have been thought to independently mediate the perception of specific somatosensory “submodalities,” such as vibration, stretch, and texture (Johnson, 2001). However, mounting evidence suggests that signals from distinct somatosensory submodalities are in fact combined in the CNS, and most tactile percepts rely on multiple submodalities (Saal and Bensmaia, 2014). For example, a recent study found that all areas of somatosensory cortex receive input from both touch and proprioceptive neurons (Kim et al., 2015).

Where in the somatosensory processing hierarchy are signals from different mechanoreceptor types first integrated? There is some anatomical evidence that this type of integration begins within the dorsal horn of the spinal cord (Abraira and Ginty, 2013; Maxwell et al., 1985). There is also functional evidence of early submodality integration—for example, some neurons in the cat spinal cord respond to both skin touch and joint movement (Wall, 1967), while neurons in the cuneate nucleus of the brainstem exhibit tactile feature selectivity that is indicative of submodality integration (Jörntell et al., 2014). In the mouse brainstem, there are neurons that receive direct convergent projections from different mechanoreceptor types that innervate the same whisker on the face (Sakurai et al., 2013). However, despite these examples, little is known about the specific sites and mechanisms of submodality integration in vertebrate somatosensation.

Our results provide an example of submodality integration at the very first stage of somatosensory processing, immediately postsynaptic to peripheral touch receptors. Specifically, we found that intersegmental neurons integrate excitatory touch signals from bristle neurons with inhibition from proprioceptive neurons in the femoral chordotonal organ. Studies of the femoral chordotonal organ in larger insects suggest that individual chordotonal neurons encode movements and static positions of the tibia (Field and Matheson, 1998). Thus, inhibitory input to ascending neurons may serve to suppress excitatory touch signals at specific phases of the walking cycle, or during grooming behavior. This reafferent signal may function in a manner analogous to corollary discharge, in which efferent motor commands are used to alter sensory signals that arise from self-generated movements (Poulet and Hedwig, 2007). Interestingly, a recent study in larval *Drosophila* found that nociceptive inputs and proprioceptive inputs can converge at the level of second-order neurons, and in this case, the interaction is summation rather than suppression (Ohyama et al., 2015). Together, these results suggest that integration across submodalities is widespread and very early in this system, consistent with the evidence in vertebrates.

### Comparison with Other Insect Species

Many features of our data are similar to previous observations in larger insects such as the locust, cockroach, and stick insect

(Burrows, 1996). For example, a single bristle on the locust leg can provide direct synaptic input to multiple classes of central neurons (Burrows, 1992), and the spatial gradients of tactile sensory input in some of these neurons resemble the receptive fields of the midline spiking neurons in our study. In addition, a study in the locust described second-order somatosensory neurons that integrate touch with signals from leg chordotonal neurons (Burrows, 1988). Another described a central neuron that integrates bristle signals from ipsilateral and contralateral legs (Nagayama, 1990). The morphologies of some of the neurons we identified resemble the morphologies of previously described locust neurons, including the ascending intersegmental neurons (Laurent and Burrows, 1988) and the midline local neurons (Burrows and Siegler, 1984).

By using genetic techniques to identify, target, and manipulate specific neuron populations, our study builds upon these previous results in several ways. First, population-level two-photon calcium imaging allowed us to estimate the total number and distribution of central neurons that process touch and to situate our results within that map. Second, optogenetic tools allowed us to fully catalog the inputs to each central neuron class from different genetically defined mechanoreceptor types and to systematically investigate how these inputs are integrated. Third, by recording from the same genetically identified neurons in multiple individuals, we were able to build up a cumulative picture of each cell class and make explicit comparisons between classes. In the future, because all these neurons are genetically identifiable, it should be possible to trace their output connections, and to identify their functional role within the broader context of sensory and motor circuits in the VNC. By combining the classic advantages of insect neurophysiology with new genetic tools, *Drosophila* should prove a useful complement to other model organisms in dissecting the fundamental mechanisms of somatosensory processing.

### EXPERIMENTAL PROCEDURES

Procedures are briefly summarized below. Details (including information on all genotypes and transgenes) are provided in the [Supplemental Experimental Procedures](#).

#### Fly Stocks

*Drosophila* were raised on standard fly food and kept on a 12-hr light/12-hr dark cycle at 25°C. All imaging and electrophysiology experiments were performed on female flies 1–3 days post-eclosion. Flies for all optogenetics experiments were raised on food supplemented with all-trans retinal.

#### CNS Electrophysiology and Imaging

A fly was fixed ventral side facing up to the underside of a thin steel platform perforated with a precision-milled hole. The ventral head and ventral thorax were partly inserted through the hole so they were accessible from above. In all experiments except for those in [Figure 7](#), the legs were glued down. The top side of the platform was perfused with oxygenated saline. A small hole was dissected in the cuticle of the ventral thorax to expose the prothoracic neuromeres. The perineural sheath under the hole was removed for electrophysiological recordings but left intact for calcium imaging. Whole-cell patch-clamp recordings were targeted to GFP-expressing neuronal cell bodies using an upright microscope with a 40× water-immersion objective. Calcium imaging was performed by expressing GCaMP6f in all neurons and recording fluorescence signals from the VNC with a custom 2-photon microscope.

### Mechanical and Optogenetic Stimulation

Bristles were mechanically stimulated with a glass pipette mounted on a piezoelectric actuator. Optogenetic stimulation of mechanoreceptors was achieved by illuminating the leg with green light (530 nm) through a fiber optic cannula. The optogenetically stimulated region encompassed 20–80 bristles, depending on its position on the leg. Although some LexA lines had expression in central neurons in the VNC (Figure S2), these cells were not directly stimulated by focal illumination of the leg. We verified that axons of passage were not activated by the stimuli we used in these experiments (Figure S6B).

### SUPPLEMENTAL INFORMATION

Supplemental Information includes Supplemental Experimental Procedures, seven figures, and one table and can be found with this article online at <http://dx.doi.org/10.1016/j.cell.2016.01.014>.

### AUTHOR CONTRIBUTIONS

J.C.T. performed the experiments and analyzed the data. J.C.T. and R.I.W. designed the experiments and wrote the manuscript.

### ACKNOWLEDGMENTS

We are grateful to Barret Pfeiffer, David Anderson, and Brian Duistermars for sharing flies prior to publication. Daryl Gohl, Marion Silies, and Tom Clandinin created the InSITE GAL4 collection and provided advice on the LexA swap. Ofer Mazon and Pavel Gorelik provided technical assistance. We thank David Ginty, Michael Dickinson, Philip Holmes, Jan Ache, and members of the R.I.W. lab for feedback on the manuscript, and Robin Harris and Andy Seeds for helpful discussions. J.C.T. is the recipient of an NRSA fellowship from the NIH (F32-NS089259). This work was partly funded by NIH grant U01-NS090514 to R.I.W. R.I.W. is an HHMI Investigator.

Received: September 21, 2015

Revised: November 23, 2015

Accepted: January 4, 2016

Published: February 25, 2016

### REFERENCES

- Abraira, V.E., and Ginty, D.D. (2013). The sensory neurons of touch. *Neuron* 79, 618–639.
- Ahn, A.N., Meijer, K., and Full, R.J. (2006). In situ muscle power differs without varying in vitro mechanical properties in two insect leg muscles innervated by the same motor neuron. *J. Exp. Biol.* 209, 3370–3382.
- Barlow, H.B. (1961). Possible principles underlying the transformation of sensory messages. In *Sensory Communication*, W.A. Rosenblith, ed. (MIT Press), pp. 217–234.
- Baek, M., and Mann, R.S. (2009). Lineage and birth date specify motor neuron targeting and dendritic architecture in adult *Drosophila*. *J. Neurosci.* 29, 6904–6916.
- Brierley, D.J., Rathore, K., VijayRaghavan, K., and Williams, D.W. (2012). Developmental origins and architecture of *Drosophila* leg motoneurons. *J. Comp. Neurol.* 520, 1629–1649.
- Brown, A.G., and Franz, D.N. (1969). Responses of spinocervical tract neurones to natural stimulation of identified cutaneous receptors. *Exp. Brain Res.* 7, 231–249.
- Burrows, M. (1988). Responses of spiking local interneurons in the locust to proprioceptive signals from the femoral chordotonal organ. *J. Comp. Physiol. A Neuroethol. Sens. Neural Behav. Physiol.* 164, 207–217.
- Burrows, M. (1992). Reliability and effectiveness of transmission from exteroceptive sensory neurons to spiking local interneurons in the locust. *J. Neurosci.* 12, 1477–1489.
- Burrows, M. (1996). *Neurobiology of an Insect Brain* (Oxford University Press).
- Burrows, M., and Siegler, M.V. (1984). The morphological diversity and receptive fields of spiking local interneurons in the locust metathoracic ganglion. *J. Comp. Neurol.* 224, 483–508.
- Chen, T.W., Wardill, T.J., Sun, Y., Pulver, S.R., Renninger, S.L., Baohan, A., Schreiter, E.R., Kerr, R.A., Orger, M.B., Jayaraman, V., et al. (2013). Ultrasensitive fluorescent proteins for imaging neuronal activity. *Nature* 499, 295–300.
- Corfas, G., and Dudai, Y. (1989). Habituation and dishabituation of a cleaning reflex in normal and mutant *Drosophila*. *J. Neurosci.* 9, 56–62.
- Corfas, G., and Dudai, Y. (1990). Adaptation and fatigue of a mechanosensory neuron in wild-type *Drosophila* and in memory mutants. *J. Neurosci.* 10, 491–499.
- Field, L.H., and Matheson, T. (1998). Chordotonal organs of insects. In *Advances in Insect Physiology*, P.D. Evans, ed. (Academic Press), pp. 1–228.
- Gohl, D.M., Silies, M.A., Gao, X.J., Bhalariao, S., Luongo, F.J., Lin, C.C., Potter, C.J., and Clandinin, T.R. (2011). A versatile in vivo system for directed dissection of gene expression patterns. *Nat. Methods* 8, 231–237.
- Harris, R.M., Pfeiffer, B.D., Rubin, G.M., and Truman, J.W. (2015). Neuron hemilineages provide the functional ground plan for the *Drosophila* ventral nervous system. *eLife* 4, 4.
- Heckscher, E.S., Zarin, A.A., Faumont, S., Clark, M.Q., Manning, L., Fushiki, A., Schneider-Mizell, C.M., Fetter, R.D., Truman, J.W., Zwart, M.F., et al. (2015). Even-skipped(+) interneurons are core components of a sensorimotor circuit that maintains left-right symmetric muscle contraction amplitude. *Neuron* 88, 314–329.
- Hengstenberg, R. (1973). The effect of pattern movement on the impulse activity of the cervical connective of *Drosophila melanogaster*. *Z. Naturforsch. C* 28, 593–596.
- Höltje, M., and Hustert, R. (2003). Rapid mechano-sensory pathways code leg impact and elicit very rapid reflexes in insects. *J. Exp. Biol.* 206, 2715–2724.
- Iwamura, Y. (2000). Bilateral receptive field neurons and callosal connections in the somatosensory cortex. *Philos. Trans. R. Soc. Lond. B Biol. Sci.* 355, 267–273.
- Jenett, A., Rubin, G.M., Ngo, T.T., Shepherd, D., Murphy, C., Dionne, H., Pfeiffer, B.D., Cavallaro, A., Hall, D., Jeter, J., et al. (2012). A GAL4-driver line resource for *Drosophila* neurobiology. *Cell Rep.* 2, 991–1001.
- Jindrich, D.L., and Full, R.J. (2002). Dynamic stabilization of rapid hexapedal locomotion. *J. Exp. Biol.* 205, 2803–2823.
- Johnson, K.O. (2001). The roles and functions of cutaneous mechanoreceptors. *Curr. Opin. Neurobiol.* 11, 455–461.
- Jörtell, H., Bengtsson, F., Geborek, P., Spanne, A., Terekhov, A.V., and Hayward, V. (2014). Segregation of tactile input features in neurons of the cuneate nucleus. *Neuron* 83, 1444–1452.
- Kim, S.S., Gomez-Ramirez, M., Thakur, P.H., and Hsiao, S.S. (2015). Multimodal Interactions between Proprioceptive and Cutaneous Signals in Primary Somatosensory Cortex. *Neuron* 86, 555–566.
- Klapoetke, N.C., Murata, Y., Kim, S.S., Pulver, S.R., Birdsey-Benson, A., Cho, Y.K., Morimoto, T.K., Chuong, A.S., Carpenter, E.J., Tian, Z., et al. (2014). Independent optical excitation of distinct neural populations. *Nat. Methods* 11, 338–346.
- Laurent, G., and Burrows, M. (1988). A population of ascending intersegmental interneurons in the locust with mechanosensory inputs from a hind leg. *J. Comp. Neurol.* 275, 1–12.
- Lundberg, A. (1979). Multisensory control of spinal reflex pathways. *Prog. Brain Res.* 50, 11–28.
- Maxwell, D.J., Koerber, H.R., and Bannatyne, B.A. (1985). Light and electron microscopy of contacts between primary afferent fibres and neurones with axons ascending the dorsal columns of the feline spinal cord. *Neuroscience* 16, 375–394.
- Merritt, D.J., and Murphey, R.K. (1992). Projections of leg proprioceptors within the CNS of the fly *Phormia* in relation to the generalized insect ganglion. *J. Comp. Neurol.* 322, 16–34.

- Murphey, R.K., Possidente, D., Pollack, G., and Merritt, D.J. (1989a). Modality-specific axonal projections in the CNS of the flies *Phormia* and *Drosophila*. *J. Comp. Neurol.* *290*, 185–200.
- Murphey, R.K., Possidente, D.R., Vandervorst, P., and Ghysen, A. (1989b). Compartments and the topography of leg afferent projections in *Drosophila*. *J. Neurosci.* *9*, 3209–3217.
- Nagayama, T. (1990). The organization of receptive fields of an antero-medial group of spiking local interneurons in the locust with exteroceptive inputs from the legs. *J. Comp. Physiol. A* *166*, 471–476.
- Niven, J.E., and Laughlin, S.B. (2008). Energy limitation as a selective pressure on the evolution of sensory systems. *J. Exp. Biol.* *211*, 1792–1804.
- Ohyama, T., Schneider-Mizell, C.M., Fetter, R.D., Aleman, J.V., Franconville, R., Rivera-Alba, M., Mensh, B.D., Branson, K.M., Simpson, J.H., Truman, J.W., et al. (2015). A multilevel multimodal circuit enhances action selection in *Drosophila*. *Nature* *520*, 633–639.
- Pick, S., and Strauss, R. (2005). Goal-driven behavioral adaptations in gap-climbing *Drosophila*. *Curr. Biol.* *15*, 1473–1478.
- Poulet, J.F.A., and Hedwig, B. (2007). New insights into corollary discharges mediated by identified neural pathways. *Trends Neurosci.* *30*, 14–21.
- Ramdy, P., Lichocki, P., Cruchet, S., Frisch, L., Tse, W., Floreano, D., and Benton, R. (2015). Mechanosensory interactions drive collective behaviour in *Drosophila*. *Nature* *519*, 233–236.
- Ridgel, A.L., Frazier, S.F., and Zill, S.N. (2001). Dynamic responses of tibial campaniform sensilla studied by substrate displacement in freely moving cockroaches. *J. Comp. Physiol. A* *187*, 405–420.
- Saal, H.P., and Bensmaia, S.J. (2014). Touch is a team effort: interplay of submodalities in cutaneous sensibility. *Trends Neurosci.* *37*, 689–697.
- Sakurai, K., Akiyama, M., Cai, B., Scott, A., Han, B.-X., Takatoh, J., Sigrist, M., Arber, S., and Wang, F. (2013). The organization of submodality-specific touch afferent inputs in the vibrissa column. *Cell Rep.* *5*, 87–98.
- Schaefer, P.L., Kondagunta, G.V., and Ritzmann, R.E. (1994). Motion analysis of escape movements evoked by tactile stimulation in the cockroach *Periplaneta americana*. *J. Exp. Biol.* *190*, 287–294.
- Seeds, A.M., Ravbar, P., Chung, P., Hampel, S., Midgley, F.M., Jr., Mensh, B.D., and Simpson, J.H. (2014). A suppression hierarchy among competing motor programs drives sequential grooming in *Drosophila*. *eLife* *3*, e02951.
- Shuler, M.G., Krupa, D.J., and Nicolelis, M.A. (2002). Integration of bilateral whisker stimuli in rats: role of the whisker barrel cortices. *Cereb. Cortex* *12*, 86–97.
- Smith, S.A., and Shepherd, D. (1996). Central afferent projections of proprioceptive sensory neurons in *Drosophila* revealed with the enhancer-trap technique. *J. Comp. Neurol.* *364*, 311–323.
- Srinivasan, M.V., Laughlin, S.B., and Dubs, A. (1982). Predictive coding: a fresh view of inhibition in the retina. *Proc. R. Soc. Lond. B Biol. Sci.* *216*, 427–459.
- Vandervorst, P., and Ghysen, A. (1980). Genetic control of sensory connections in *Drosophila*. *Nature* *286*, 65–67.
- Wall, P.D. (1967). The laminar organization of dorsal horn and effects of descending impulses. *J. Physiol.* *188*, 403–423.
- Zill, S., Schmitz, J., and Büschges, A. (2004). Load sensing and control of posture and locomotion. *Arthropod Struct. Dev.* *33*, 273–286.

## A *Drosophila* leg mechanoreceptors

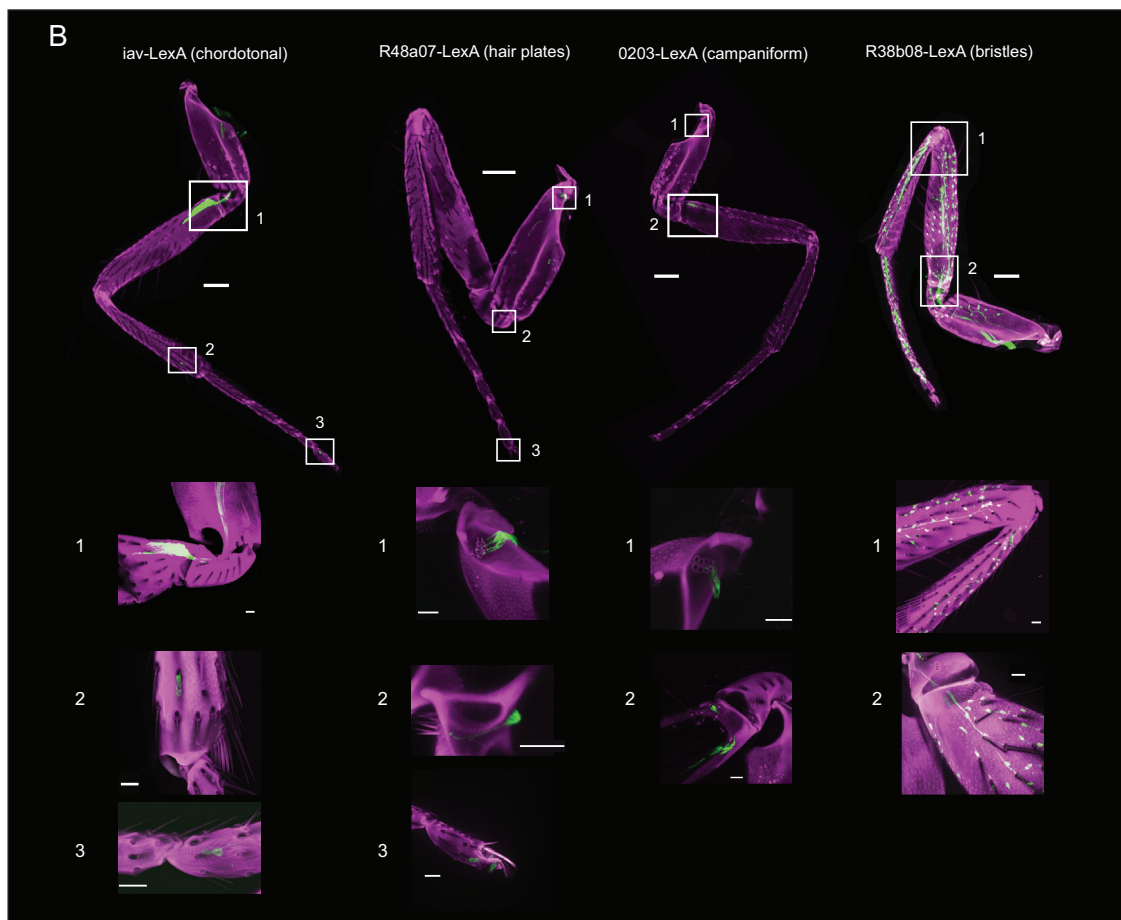
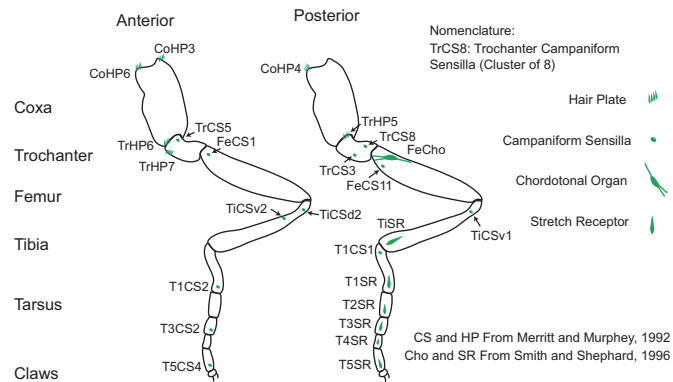


**Figure S1. LexA Lines Targeting Fly Leg Mechanoreceptors, Related to Figure 1**

(A) Map of proprioceptors on the *Drosophila* leg. For clarity, bristles are not shown.

(B) A projection of a confocal stack through a prothoracic leg for each LexA line used to target peripheral mechanoreceptors. The magenta channel is cuticle autofluorescence (imaged at 633 nm) and green is expression of UAS::mCD8-GFP (imaged at 488 nm), driven by LexA. Shown below are higher magnification images corresponding to specific regions of the leg, Magnified images are not necessarily taken from the same fly, but expression was consistent across flies. We observed no GFP expression in muscles. Scale bars are 100  $\mu$ m for whole legs and 20  $\mu$ m for magnified images below.

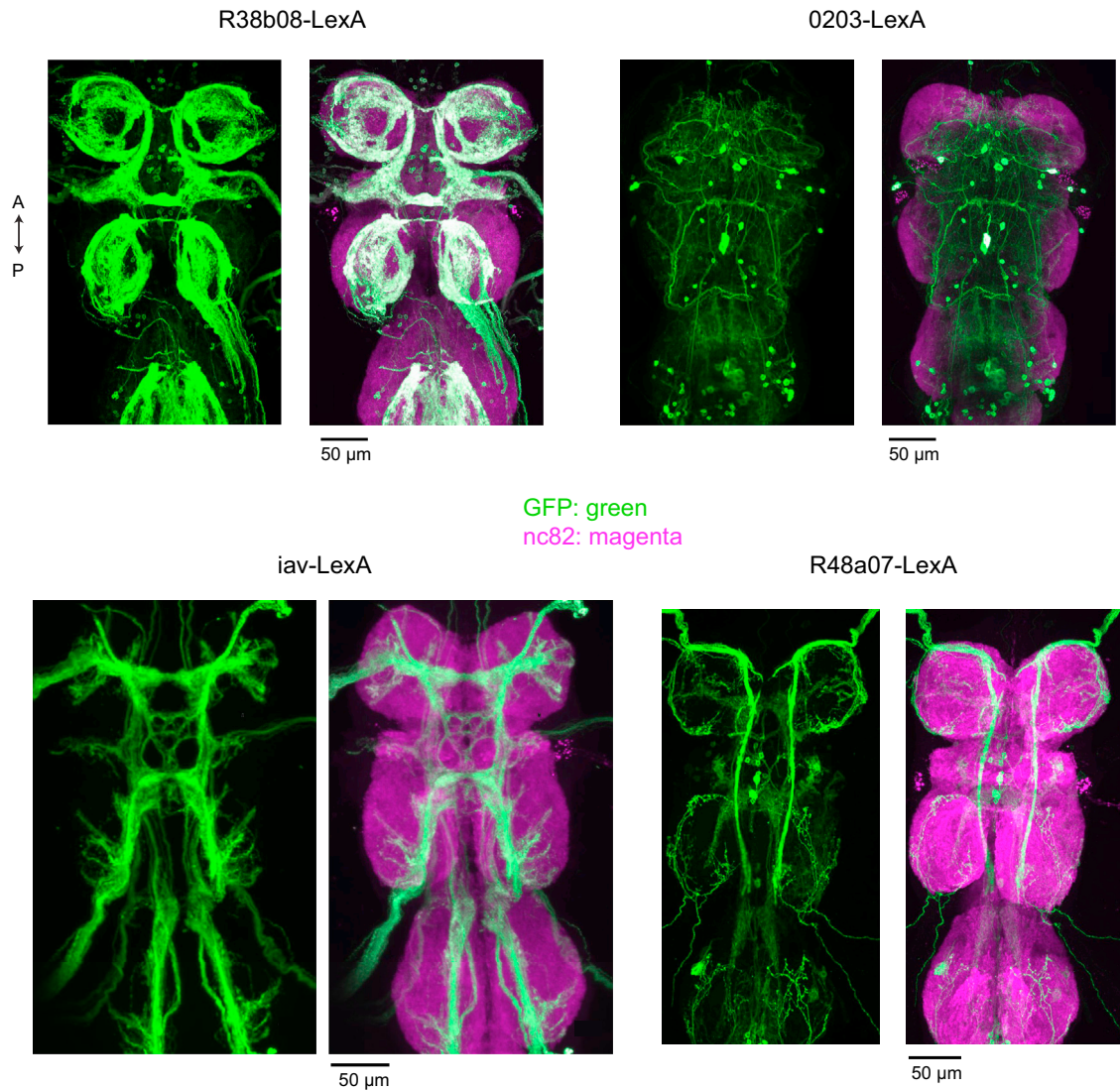


**Figure S2. Central Expression of Sensory LexA Lines, Related to Figure 1**

Anatomy of LexA lines labeling leg mechanoreceptor neurons. Shown at left are coronal maximum intensity projections of mCD8::GFP expression amplified with anti-CD8 antibody (green), and an antibody against the neuropil marker bruchpilot (nc82) shown in magenta. All lines except iav-LexA have expression in many central neurons. However, central neurons will not be excited by our optogenetic stimuli, because our stimuli consisted of focal spots of light directed at the legs.

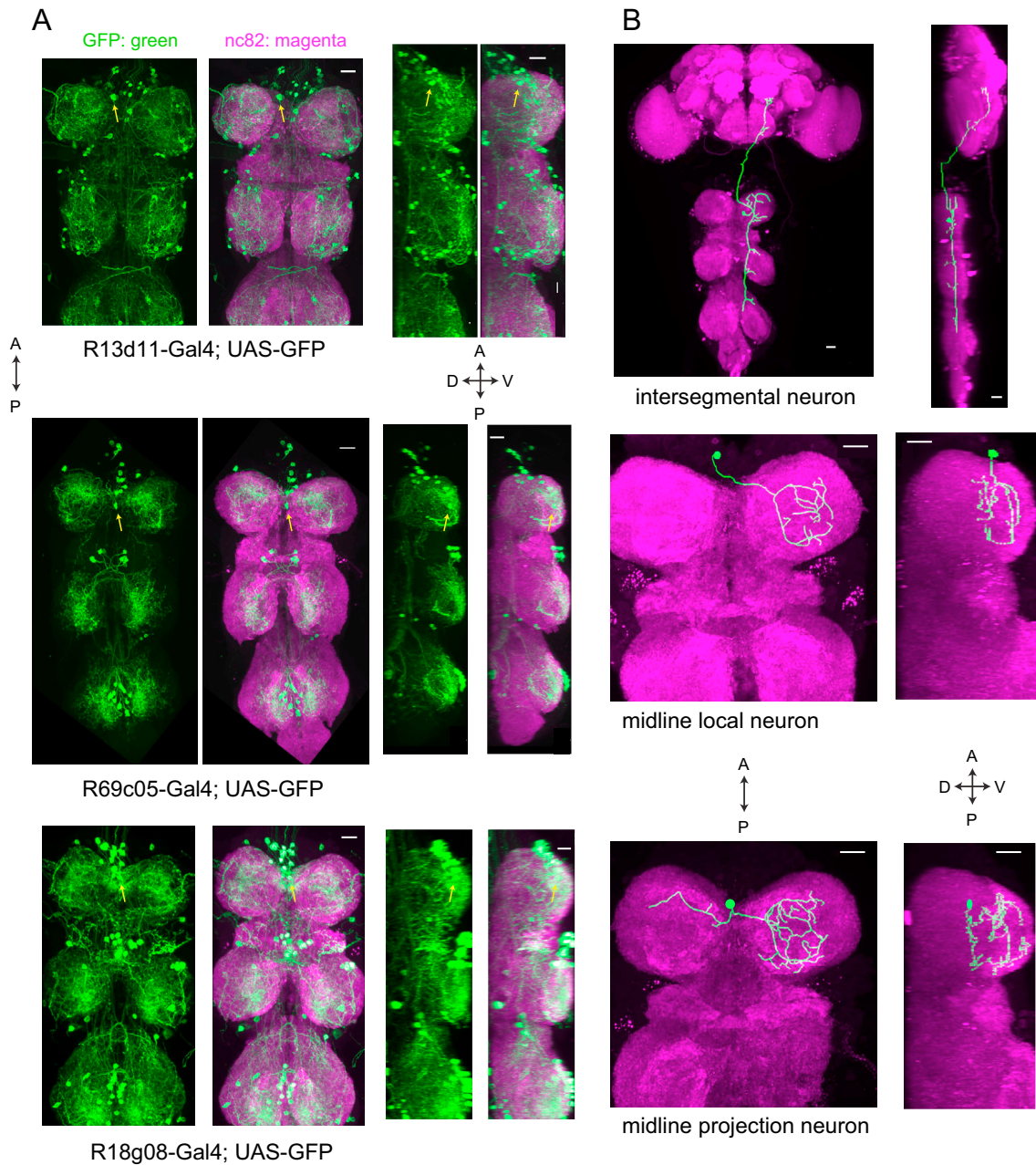


**Figure S3. Population and Single Neuron Anatomy of Three Second-Order Neuron Classes, Related to Figures 3, 4, 5, and 6**

(A) Anatomy of GAL4 lines labeling central neurons. Shown at left are coronal maximum intensity projections of mCD8::GFP expression amplified with anti-CD8 antibody (green), and an antibody against the neuropil marker bruchpilot (nc82) shown in magenta. The two images at the right show sagittal projections of the same VNC. Yellow arrows indicate the position of typical cell bodies which were targeted for electrophysiological recordings. Scale bars, 50  $\mu$ m.

(B) Anatomy of single neurons from each class. Shown in green are projections of reconstructed biocytin fills from each neuron class, and in magenta, staining using an antibody against the neuropil marker bruchpilot (nc82). Because cell bodies are typically removed after the recording, cell bodies are here drawn manually to depict their approximate size and location. Scale bars, 20  $\mu$ m.

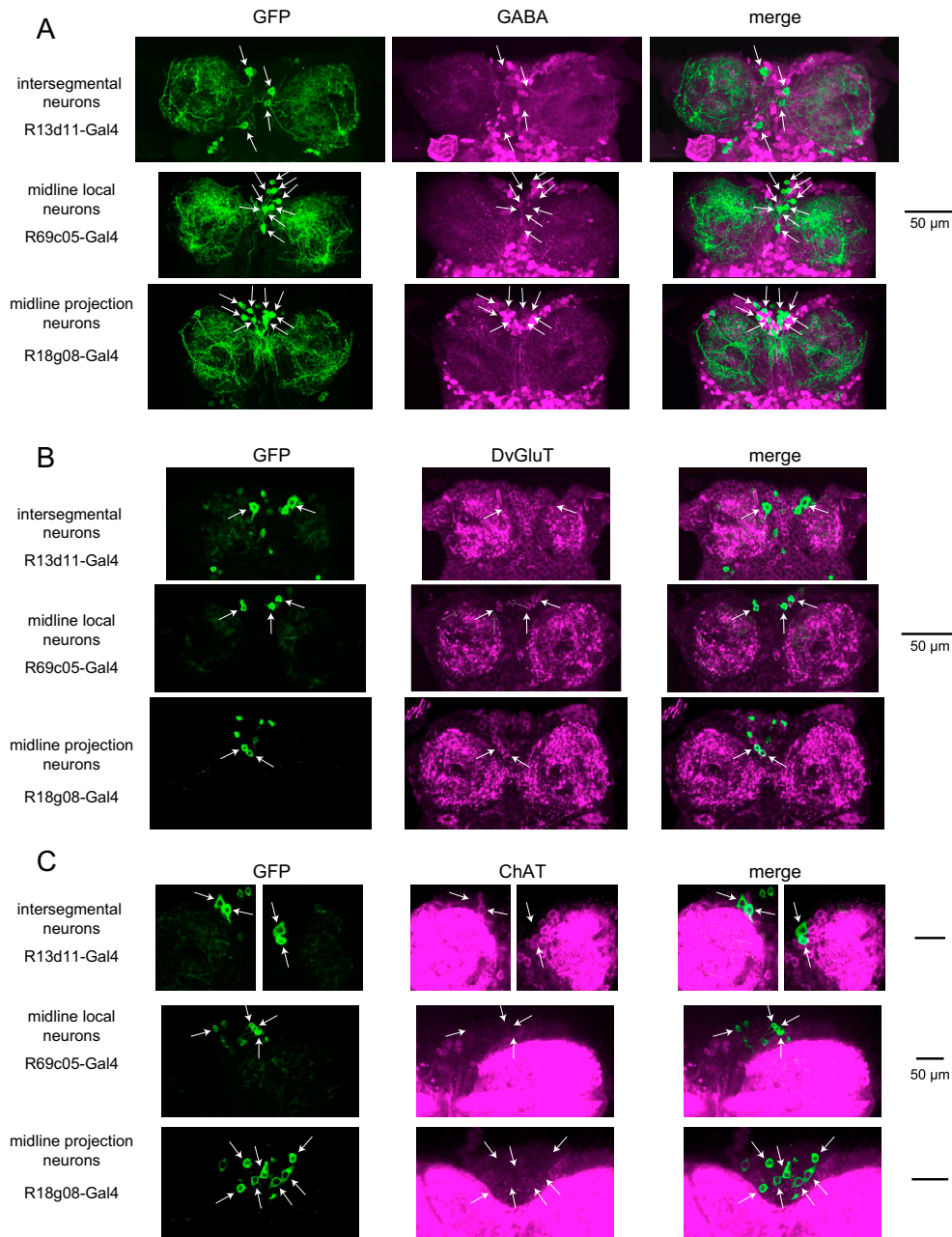


**Figure S4. Neurotransmitter Phenotypes of Central Neuron Classes, Related to Figures 3, 4, 5, and 6**

(A) Projections of confocal stacks through the ventral prothoracic VNC. Neurons labeled with antibodies against GABA are shown in magenta. Central neurons of interest are labeled with mCD8::GFP, which was amplified with an anti-CD8 antibody (green). Each channel is shown individually in the left columns, and merged on the right. White arrows indicate cell bodies belonging to the classes that we focus on in this study; cell bodies not marked with an arrow belong to other cell classes. None of the neurons indicated with white arrows are positive for GABA. We note that some GFP-expressing neurons belonging to other cell classes (e.g., the most anterior cells in R18g08) are immunopositive for GABA.

(B) Confocal projections of staining with an antibody against the *Drosophila* vesicular neurotransmitter transporter (DvGluT; magenta). As above, central neurons of interest are labeled with mCD8::GFP, which was amplified with an anti-CD8 antibody (green). Midline local (R69c05-GAL4) and midline projection (R18g08-GAL4) neurons were immunopositive for DvGluT, indicating that they release glutamate as a neurotransmitter.

(C) Confocal sections of staining with an antibody against choline acetyltransferase (ChAT; magenta). Here, the green channel represents native GFP fluorescence, which was not amplified with an antibody. The 2 separate images in the top row are from two different confocal sections within the same VNC. Within each lateral pair of intersegmental neurons, one cell was positive for ChAT; the same result was also observed in one additional VNC. For midline local and projection neurons, none of the relevant cells (indicated with white arrows) stained positive for ChAT.

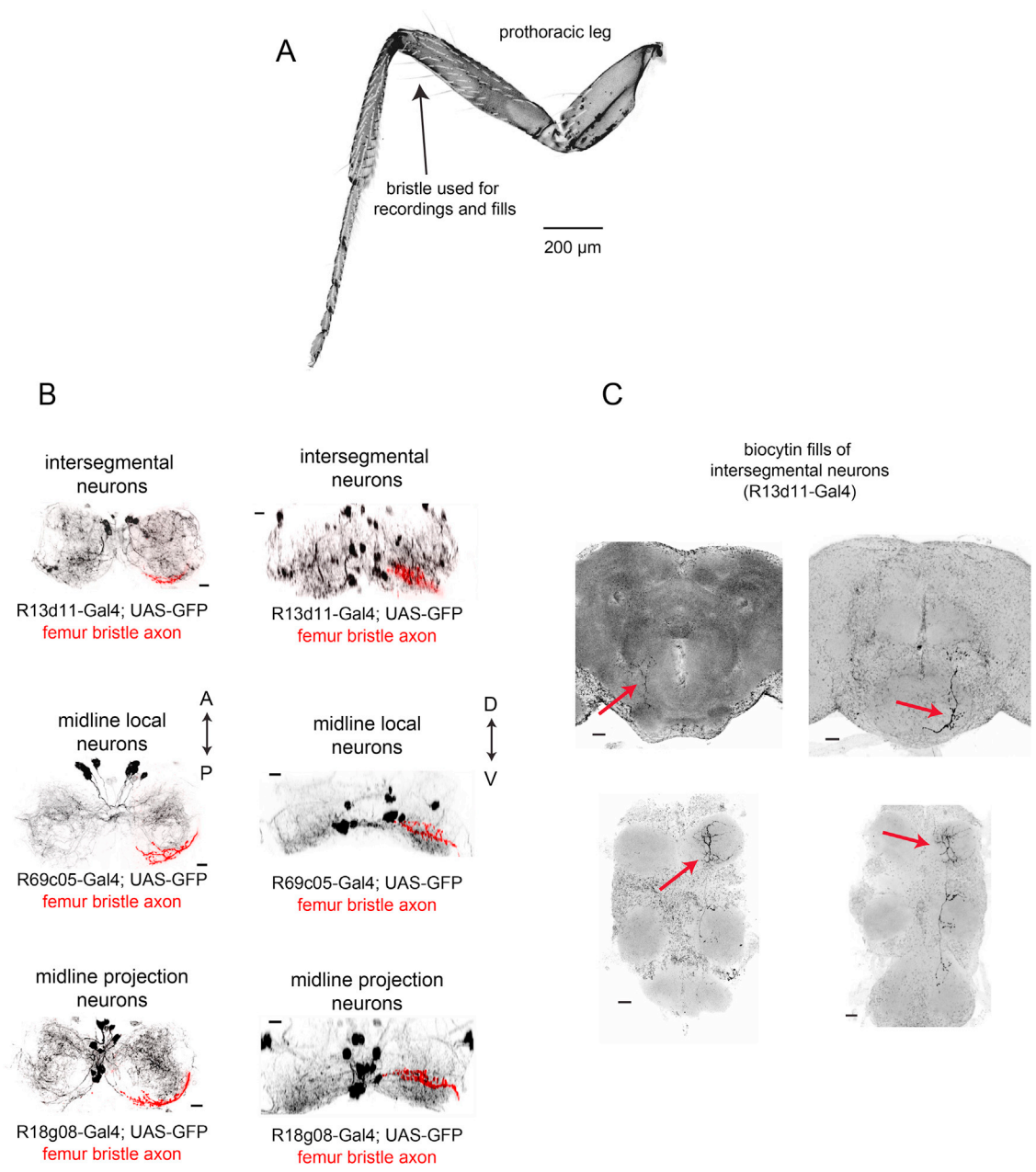


**Figure S5. Detailed Anatomy of Single Neuron Fills, Related to Figures 3 and 4**

(A) Projection of a confocal stack through the prothoracic leg, showing autofluorescence; arrow indicates the bristle used for the bristle-neuron dye-fill experiments in Figure 3, as well as all the bristle neuron recordings throughout the manuscript.

(B) Dual labeling of a bristle axon and postsynaptic neurons in the VNC. The left column shows data reproduced from Figure 3A: maximum intensity projections of GFP expression within the prothoracic neuromere of the VNC (black), co-labeled with the axonal arbor of a single femur bristle neuron filled with Dil. At right are transverse projections of the same image stacks, which demonstrate that bristle axons arborize along the ventral edge of the neuropil, where they overlap with central neuron processes. Scale bars, 10 μm.

(C) Biocytin fills of two intersegmental neurons from the same side of the VNC. One cell projects to the contralateral brain, the other projects to the ipsilateral brain. Scale bars, 20 μm.

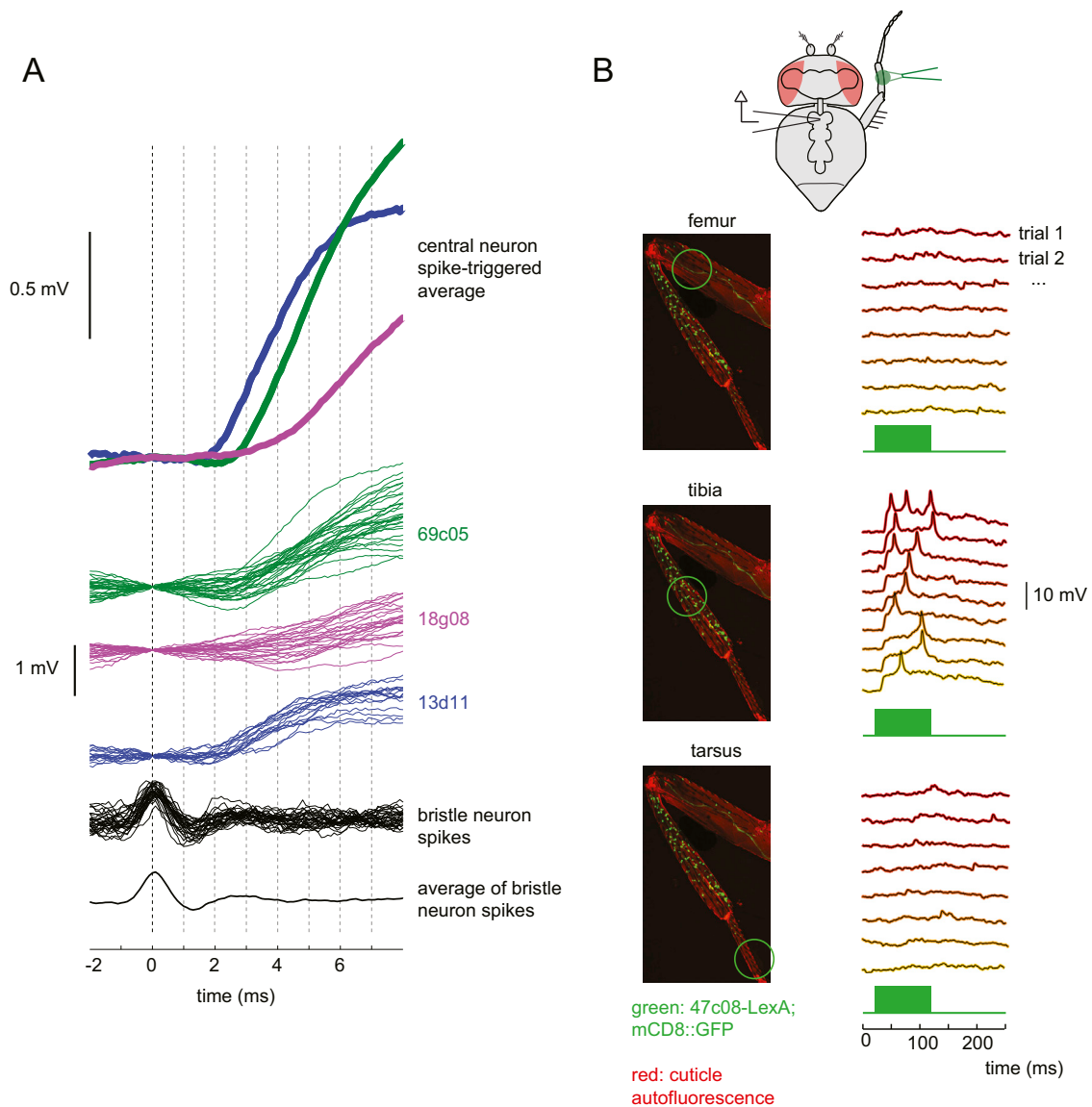


**Figure S6. Response Latency and Optogenetic Stimulation of Axons of Passage, Related to Figures 4, 5, and 6**

(A) Paired recordings from a femur bristle and central neurons in the VNC. For each central neuron class, example bristle-spike-triggered postsynaptic potentials from a single neuron are shown, with spike-triggered averages for each of those three example neurons plotted above on an expanded voltage scale. Bandpass-filtered bristle neuron spikes (as in Figure 3) are shown in black, with the average plotted below. The latency from the peak of the bristle neuron spike to the first visible depolarization is  $\sim 3$  ms. The distance from the femur bristle (Figure S5A) to the VNC is approximately  $850 \mu\text{m}$ , suggesting that the conduction velocity is  $\sim 280 \mu\text{m}/\text{ms}$ , or  $0.28 \text{ m/s}$ , assuming a negligible delay for synaptic transmission.

(B) Example recording from an intersegmental neuron while optogenetically stimulating bristle neuron axons. The line used to drive Chrimson (47c08-LexA) had LexA expression mainly in tibia bristle neurons, and in very few femur and tarsus bristle neurons. Optogenetically stimulating the distal femur, in a region where no bristle neuron cell bodies expressed Chrimson, evoked no response in the downstream neurons (top row). Because the axons of tibia bristle neurons pass through the region of femur stimulation, this indicates that Chrimson-expressing axons of passage are not activated at the light levels used in these experiments. In contrast, stimulation of tibia bristle neuron cell bodies evoked a robust response (middle row). Similar results were obtained in a total of 2 experiments. The genotype is: 47c08-LexA (attp40)/pJFRC7-20XUAS-IVS-mCD8::GFP (attp40);13d11-Gal4 (attp2)/13XLexAop2-IVS-Syn21-Chrimson::tdT-3.1-p10-F8 (VK00005).

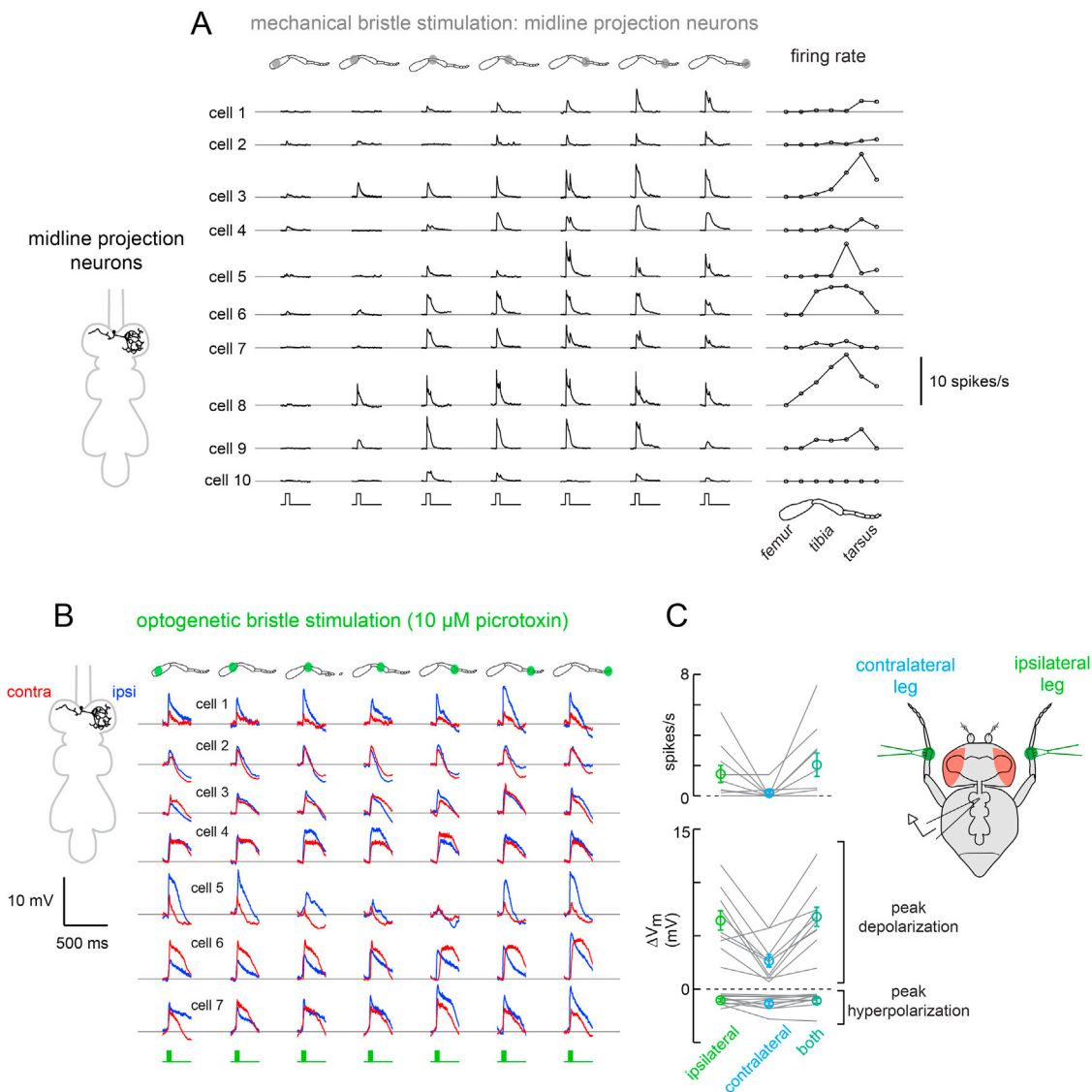


**Figure S7. Mechanical and Optogenetic Receptive Field Mapping of Midline Projection Neurons, Related to Figure 6**

(A) Trial-averaged voltage responses of midline projection neurons to mechanical stimulation of 1-2 bristles ( $n = 10$ ). These cells were not filled; rather, the neuron's orientation was predicted based on initial cell body position, and only the putative ipsilateral receptive field was measured. Trial-averaged spike rates are shown at right.

(B) Trial-averaged voltage responses of midline projection neurons to optogenetic stimulation of bristle neurons, while blocking inhibition with 10  $\mu$ M picrotoxin. These experiments ( $n = 7$ ) are a subset of those shown in Figure 6A. For each neuron, responses were measured for both the ipsilateral (blue) and contralateral (red) prothoracic legs.

(C) Population data for bilateral stimulation experiments (Figure 6C). Trial-averaged spike rates and peak membrane potential deflections are shown for each neuron ( $n = 10$ ).

**Cell, Volume 164**

**Supplemental Information**

**Parallel Transformation of Tactile Signals  
in Central Circuits of *Drosophila***

**John C. Tuthill and Rachel I. Wilson**

## Supplemental Experimental Procedures

### Fly Stocks

*Drosophila* were raised in sparse cultures on standard cornmeal agar medium supplemented with rehydrated potato flakes (Carolina Biological Supply), and kept on a 12-h light, 12-h dark cycle at 25° C. All imaging and electrophysiology experiments were performed on female flies 1-3 days post-eclosion. Flies for all optogenetics experiments were raised on food supplemented with all-trans retinal (all-trans-retinal was prepared as a 35 mM solution in ethanol, and 100 ml of this solution was mixed into a layer of rehydrated potato flakes approximately 0.5 cm deep in a standard 6-oz culture bottle). Descriptions of all fly stocks used in the study are listed in the Table of Transgenes. The genotypes used, by figure, are listed in the Table of Genotypes. Both of these tables are appended to the end of this section.

### Electrophysiology

Whole-cell patch clamp recordings were performed as previously described (Wilson et al., 2004), with some modifications. Flies were cold-anesthetized and fixed to the underside of a custom-milled steel platform (0.001" thickness). The fly was mounted with its ventral side facing up, using UV-cured glue (KOA 300, Kemxert). The ventral head and anterior thorax were partly inserted through a hole in the platform. Thus, both the ventral head and a small part of the ventral thorax (from the neck connective to the base of the mesothoracic legs) were visible and accessible from above. The top side of the platform, and thus also the exposed parts of the head and thorax, were continually perfused with oxygenated saline. In all experiments except for those in Figure 7, all six legs were glued to the holder with UV-cured glue. A small hole was manually dissected in the cuticle of the ventral thorax to expose the prothoracic neuromeres, and the perineural sheath was gently removed with fine forceps to expose neuronal cell bodies.

The saline which perfused the preparation contained: 103 mM NaCl, 3 mM KCl, 5 mM TES, 8 mM trehalose, 10 mM glucose, 26 mM NaHCO<sub>3</sub>, 1 mM NaH<sub>2</sub>PO<sub>4</sub>, 1.5 mM CaCl<sub>2</sub>, and 4 mM MgCl<sub>2</sub> (pH 7.1, osmolality adjusted to 270-275 mOsm). The saline was bubbled with 95% O<sub>2</sub>/5% CO<sub>2</sub> and was perfused at ~2-3 ml/min. Recordings were performed at room temperature. Cell bodies were visualized using an infrared LED (Smartvision) and a 40× water-immersion objective on an upright compound microscope equipped with a fluorescence attachment (Olympus BX51F).

Whole-cell patch-clamp recordings were targeted to GFP-labeled cell bodies in the prothoracic region of the VNC. The internal patch pipette solution contained (in mM): 140 potassium aspartate, 10 HEPES, 1 EGTA, 4 MgATP, 0.5 Na<sub>3</sub>GTP, 1 KCl, and 13 biocytin hydrazide (pH 7.2, osmolality adjusted to ~265 mOsm). Although there were other VNC neurons labeled by each Gal4 line (Figure S3A), it was easy to distinguish the target neurons from the other neurons by the characteristic and reliable positions of their cell bodies, as well as their intrinsic properties: recorded neurons in each class had a characteristic input resistance, resting membrane potential, and spike waveform. We were able to reliably record from midline local and projection neurons by targeting the most ventral cell bodies along the midline in each GAL4 line. We targeted intersegmental neurons based on their large cell body size and characteristic position. Typical positions of target neuron cell bodies are indicated in Figure S3A.

All recordings were made in current-clamp mode using an Axopatch 200B amplifier. Data were low-pass filtered at 5 kHz before they were digitized at 10 kHz by a 16 bit A/D converter (National Instruments, USB-6343), and acquired in Labview. Stable recordings were typically maintained for 1-2 hours. A small hyperpolarizing current (approximately -5 to -10 pA) was injected to compensate for the depolarizing seal conductance (Gouwens and Wilson, 2009). Analysis of electrophysiology data was performed with custom scripts written in MATLAB and Python.

For all bristle recordings displayed, the second-most distal bristle on the posterior surface of the femur (Figure S5A) was manually clipped with fine forceps to approximately 25% of its full length. We chose this bristle because it is among the largest on the prothoracic leg (Hannah-Alava, 1958), and we found it more difficult to record spikes from smaller bristles. To record bristle neuron signals, a glass recording pipette was inserted over the cut bristle tip. The recording electrode was filled with a high K<sup>+</sup> saline that was identical to the external saline except for the concentrations of NaCl (9 mM) and KCl (121 mM). This solution was designed to mimic the high K<sup>+</sup> concentration of the mechanoreceptor lymph (Grunert and Gnatzy, 1987; Thurm and Kuppers, 1980), and has previously been shown to effectively preserve the bristle's trans-epithelial potential and mechanosensory responses (Kernan et al., 1994). Bristle recordings were band-pass filtered using a 2<sup>nd</sup> order Butterworth filter with cutoff frequencies of 100 and 400 Hz. In all bristle recordings, the recorded spike amplitude was greater at high firing rates (e.g., Figure 2A).

### Mechanical and Optogenetic Stimulation

Bristles were mechanically stimulated with a closed-loop piezoelectric actuator (Physik Instrumente P-841.60, 90 μm travel range, with E-509.S1 sensor/piezo servo-control module). The bristle recording electrode consisted of a glass capillary which was mounted on the actuator with a custom-milled aluminum holder, which held the capillary firmly in place with a

set screw. A recording wire was fixed to the interior of the pipette with a rubber gasket (Axon Instruments) and connected to the headstage by 6 inches of flexible shielded wire. Extracellular bristle signals were acquired in zero-current ( $I=0$ ) mode with an Axon 200B patch-clamp amplifier, and digitized at 10 kHz. The same basic configuration was used for recording bristle neuron spikes (Figure 2 and Figure 3) and also for simply deflecting the bristles without recording from the bristle neurons (Figures 4-7); the only difference was that in the latter configuration the recording wire was not inserted into the glass capillary.

Insect bristles are directionally selective—they respond most strongly to deflection in a particular direction, which depends on the asymmetric orientation of the hair socket (Burrows, 1996; Corfas and Dudai, 1990). For all bristle recordings in this study, we restricted the stimulus to movement in the bristle’s preferred direction, i.e. the direction that reduced the acute angle between the bristle and the cuticle.

Optogenetic stimuli were delivered to the leg with a fiber optic cannula (0.22 NA, Thorlabs) coupled to a green LED driver (530 nm; Smartvision S-30). We used a fiber optic cannula with a 50  $\mu\text{m}$  core (Thorlabs) in all experiments except the GCaMP imaging experiments in Figure 2C-G, where we used a cannula with a 200  $\mu\text{m}$  core. For the experiments in Figures 2A, 2C-G, 4A, 5A, and 6A, the stimuli were 100 ms light pulses. For the experiments in Figures 4D-E and 5D-E, the light stimuli were 500 ms light pulses, and in Figure 6C, 200 ms and 500 ms stimuli were used. All light stimuli were delivered at 5 kHz with a 40% duty cycle, and the LED was powered at 40% of its maximum output. The diameter of the effective light spot at the sample, measured by recording from a bristle and sequentially moving the fiber optic away from the recording site, was approximately 200  $\mu\text{m}$ , encompassing 20-80 bristles, depending on the location on the leg (Hannah-Alava, 1958). Although some LexA lines had expression in central neurons in the VNC (Figure S2), these cells were not directly stimulated by focal illumination of the leg. We verified that axons of passage were not activated by the stimuli we used in these experiments (Figure S6B).

Mechanical and optogenetic stimuli were generated in Labview and sent to the amplifier at 5 kHz using a separate analog output DAQ (National Instruments 9263). The positions of the recording/stimulation electrode and the fiber optic were controlled with separate servo-controlled XYZ translation stages (Thorlabs) and custom Labview software. The fly’s leg, as well as the mechanical and optical probes, were visualized with a camera positioned below the stage (Point Grey Firefly) coupled to a 50 $\times$  air objective (Olympus). The camera and objective were also mounted on servo-controlled translation stages, to visualize the stimulus probes and the surface of the fly’s leg.

### Calcium Imaging

The experimental preparation for calcium imaging was essentially the same as for electrophysiological recordings, except that the sheath was left intact and the fly’s esophagus and crop were removed to prevent movement. GCaMP6f was expressed in all neurons under Gal4/UAS control, and Chrimson was expressed specifically in leg bristle neurons under LexA/LexAOp control (genotype: *UAS-GCaMP6f/R38b08-LexA;R57c10-Gal4/LexAop-Chrimson::TdTomato*). The optogenetic stimulus was centered on the femur/tibia joint of the fly’s left leg (for details see Mechanical and Optogenetic Stimulation, above).

Images were acquired in framescan mode on a custom built two-photon microscope using ScanImage 3.8 software (Polgruto et al., 2003), with excitation light at 925 nm. Each trial comprised 53 frames (512 $\times$ 512 pixels) imaged at 1.93 Hz, scanning from top the left of each frame to bottom right, with 5 stimuli delivered at 4 sec intervals. A single trial was captured at each z-plane, starting at  $z=0$   $\mu\text{m}$  at the ventral surface of the VNC, and progressing dorsally to  $z=-400$   $\mu\text{m}$ , in 10  $\mu\text{m}$  steps. There was a 30 sec gap between each trial. We observed spontaneous neural activity throughout the course of the experiment, indicating that the fly remained healthy and responsive.

Within each trial, all pixels from the frame containing the light artifact from the LED stimulus were set to the baseline intensity. A Gaussian low-pass filter of 5 $\times$ 5 pixels was then applied, and data from each trial were aligned in the  $xy$  plane on a frame-by-frame basis using efficient subpixel motion registration (Guizar-Sicairos et al., 2008). ROIs were manually segmented within each imaging plane to identify individual neuronal cell bodies. ROIs in adjacent z-planes with greater than 50%  $xy$  overlap were considered to be part of the same neuron. For each neuron that spanned multiple z planes, only the largest 2-D ROI (within a single z-plane) was included for subsequent analysis. Neurons with a cell body area of greater than 49  $\mu\text{m}^2$  ( $\sim 8$   $\mu\text{m}$  diameter) were classified as motor neurons.

Calcium signals ( $\Delta F/F$ ) were measured as changes in fluorescence ( $\Delta F$ ) normalized to the fluorescence during the baseline period ( $F$ , average of the 4 lowest-intensity frames in each trial.). Cross correlation of stimulus and cellular calcium signal vectors was performed for each imaging trial ( $n = 53$  frames) using the *xcov* function in MATLAB, and normalizing by the standard deviations of the stimulus and cellular calcium signal vectors. For all analyses in Figure 2, we define the stimulus correlation as the mean of the sample correlations across two lag values (+1, +2 frames). Values for the correlation between the stimulus waveform and the  $\Delta F/F$  waveform were typically less than 0.5 because the stimulus was brief (<1 frame

every 4 sec), while calcium signals typically persisted across multiple frames, either due to sustained activity or the intrinsically slow kinetics of GCaMP.

To compare whether the response of a neuron was correlated with the bristle stimulus at a level above chance, we carried out a permutation test. We again computed the cross-correlation of stimulus and cellular calcium signals, with the difference that individual time points of the stimulus vector were randomly shuffled. This procedure was repeated 1000 times for each neuron to obtain a null distribution of correlation values (Figure 2F, bottom histogram); the confidence intervals indicated in Figure 2 were calculated from this null distribution. The correlation threshold varied slightly depending on whether we shuffled the stimulus vectors (0.19), cellular calcium signal vectors (0.15), or both stimulus and cellular calcium signal vectors (0.16). Overall, the three shuffling procedures produced qualitatively similar results, but we selected the most stringent threshold as a conservative estimate of the number of neurons in the prothoracic VNC responding to bristle stimulation.

### Paired Whole-cell Recordings

In Figure 7, we targeted paired whole-cell recordings to distinct central neuron types by labeling both cell populations with GFP (genotype: *pJFRC7-20XUAS-IVS-mCD8::GFP;R13d11-Gal4/R18g08-Gal4* or *R69c05-Gal4*). During the recording, the fly's activity was recorded at 30 fps with a video camera (Point Grey Firefly) equipped with a compact long-working-distance magnifying lens (Infinistix 94 mm/1.00x) mounted under the recording stage. Fly movement was computed as the sum of absolute pixel intensity differences across adjacent video frames, normalized to the peak value in the corresponding experiment. For the activity traces in Figure 7, movement was computed for a region of interest that encompassed the fly's prothoracic leg, though the fly's other legs and abdomen occasionally entered this region.

### Pharmacology

Drugs were bath applied via the saline perfusate. Tetrodotoxin (TTX) was prepared as a concentrated stock solution in sodium citrate, CGP54626 was prepared as a concentrated stock solution in dimethyl sulfoxide, picrotoxin was prepared as a concentrated stock solution in aqueous NaCl (140 mM), and methyllycaconitine (MLA) was prepared as a stock solution in water. For the midline local neurons and the midline projection neurons (Figures 5 and 6), 10  $\mu$ M picrotoxin was sufficient to block inhibitory responses. For the intersegmental neurons (Figure 4), 100  $\mu$ M picrotoxin and 50  $\mu$ M CGP54626 was required to block inhibition. The requirement for CGP54626 implies a role for GABA<sub>B</sub> receptors (Wilson and Laurent, 2005), and the need for a higher concentration of picrotoxin suggests a role for GluCl receptors (Liu and Wilson, 2013).

Central neuron responses to bristle stimulation were completely eliminated after blocking voltage-gated sodium channels with TTX (1  $\mu$ M), as we would expect if they depended on spikes in bristle neurons. The same effect was observed with the nicotinic acetylcholine receptor antagonist methyllycaconitine (MLA, 1  $\mu$ M). This latter result implies that bristle neurons are cholinergic, like most insect mechanoreceptor neurons (Burrows, 1996). This result is contrary to previous reports suggesting that histamine is the bristle neuron neurotransmitter (Buchner et al., 1993; Melzig et al., 1996; Melzig et al., 1998). Iontophoresis of histamine into the neuropil evoked no response in intersegmental neurons, while acetylcholine iontophoresis evoked large depolarizing responses (data not shown). In addition, histamine receptor antagonists (100  $\mu$ M pyrilamine and 200  $\mu$ M cimetidine) did not have a reliable effect on the responses of intersegmental neurons to mechanical stimulation of femur bristles, whereas these responses were blocked by the nicotinic antagonist methyllycaconitine (MLA, 1  $\mu$ M). Bath application of histamine (1 mM) increased the input resistance of intersegmental neurons, suggesting a neuromodulatory effect.

### Immunohistochemistry and Anatomy

Immunohistochemistry was performed using established methods (Wilson and Laurent, 2005). Brains and VNCs were dissected and fixed for 15 min at room temperature in 4% paraformaldehyde, then rinsed in phosphate buffered saline (PBS) and incubated in blocking solution (5% goat serum in PBS + 0.2% Triton X-100 [PBST]). They were then incubated in blocking solution with primary antibodies for 24 hours at room temperature, followed by washing in PBST and incubation in blocking solution containing secondary antibodies for 24 hours at room temperature. Samples were rinsed with PBST, mounted in Vectashield, imaged on an Olympus FV1200 confocal, and analyzed in Fiji (Schindelin et al., 2012). To reconstruct the morphology of single neurons (Figures 3A and S3B), we manually traced the skeleton of each biocytin-filled neuron using the Simple Neurite Tracer plugin in Fiji. We used the Fill out command to generate a three-dimensional volume of the neuron, which was subsequently converted to a z-projection (Figures 3A and S3B).

To visualize the morphology of each biocytin-filled neuron in the context of the surrounding neuropil, the primary antibody solution contained mouse nc82 (1:50, Developmental Studies Hybridoma Bank), and the secondary antibody solution contained Alexa Fluor 568 conjugated to streptavidin (1:1000, Life Technologies) and Alexa Fluor 633 goat anti-mouse (1:250, Life Technologies), again in blocking solution. For anti-GABA immunostaining, the primary antibody solution contained mouse nc82 (1:40, Developmental Studies Hybridoma Bank), rat anti-CD8 (1:50 Life Technologies), and rabbit anti-GABA (1:100, Sigma), and the secondary antibody solution contained Alexa Fluor 633 goat anti-mouse (1:250,

Life Technologies), Alexa Fluor 568 goat anti-rabbit (1:250, Life Technologies), and Alexa Fluor 488 goat anti-rat (1:250, Life Technologies). For anti-DvGluT immunostaining, the primary antibody solution contained rabbit DvGluT (1:5000, gift of A. DiAntonio, (Daniels et al., 2008)) and rat anti-CD8 (1:50 Life Technologies), and the secondary antibody solution contained Alexa Fluor 568 goat anti-rabbit (1:250, Life Technologies), and Alexa Fluor 488 goat anti-rat (1:250, Life Technologies). For anti-ChAT immunostaining, the primary antibody solution contained mouse ChAT4B1 (1:100, Developmental Studies Hybridoma Bank, (Takagawa and Salvaterra, 1996) and the secondary antibody solution contained Alexa Fluor 633 goat anti-mouse (1:250, Life Technologies).

In Figure 3A, femur bristles were dye-filled using established techniques for labeling thoracic bristles (Kays et al., 2014), with slight modifications. Briefly, female flies were decapitated and glued to insect pins, with the prothoracic legs glued in an extended position. A single femur bristle was plucked with fine forceps from the leg of each fly, and flies were fixed overnight in 4% paraformaldehyde in 0.2 M carbonate-bicarbonate buffer at 4° C. Bristles sockets were filled with Dil dye (Life Technologies; 32 µg/µl in ethanol) using a micromanipulator-mounted pipette, during which time the flies were immersed in 0.2 M carbonate-bicarbonate buffer for 72 hours at room temperature, with the dye-filled bristle socket resting above the buffer. VNCs were then dissected and imaged as described above.

**Table of Transgenes**

Genotype	Purpose	Source
R38b08-LexA (attp40)	Leg bristle neurons/ Mechanosensory neurons innervating chemosensory bristles	(Jenett et al., 2012)
R48a07-LexA (attp40)	Trochanter/Femur Hair plates, unknown cells in the distal tarsus	(Jenett et al., 2012)
0203-LexA (III)	Femur/coxa campaniforms, some femoral chordotonal neurons	(Gohl et al., 2011), generated by J.C.T. using InSITE swap into 0203-Gal4 (PBac{IS. - LexA}0203)
iav-LexA (VK00013)	Femoral and tibial chordotonal organs	(Shearin et al., 2013)
R13d11-Gal4 (attp2)	Intersegmental neurons	(Jenett et al., 2012)
R18g08-Gal4 (attp2)	Midline projection neurons	(Jenett et al., 2012)
R69c05-Gal4 (attp2)	Midline local neurons	(Jenett et al., 2012)
nsyb-Gal4 (attp2), also known as (R57c10-Gal4)	Pan-neuronal	(Jenett et al., 2012)
ChAT-Gal4.7.4 (II)	Cholinergic neurons	(Salvaterra and Kitamoto, 2001)
pJFRC7-20XUAS-IVS-mCD8::GFP (attp2)	GFP for patching and confocal imaging	(Pfeiffer et al., 2010)
pJFRC7-20XUAS-IVS-mCD8::GFP (attp40)	GFP for patching and confocal imaging	(Pfeiffer et al., 2010)
pJFRC15-13XLexAop2-mCD8::GFP (attp2)	GFP for confocal imaging of peripheral neurons	(Pfeiffer et al., 2010)
13XLexAop2-IVS-Syn21-Chrimson::tdT-3.1-p10-F8 (VK00005)	For optogenetic mechanoreceptor stimulation	gift of Barret Pfeiffer and David Anderson (Klapoetke et al., 2014; Pfeiffer et al., 2010; Pfeiffer et al., 2012)
13XLexAop2-IVS-Syn21-Chrimson::tdT-3.1-p10-F8 (su(Hw)attP5)	For optogenetic mechanoreceptor stimulation	gift of Barret Pfeiffer and David Anderson (Klapoetke et al., 2014; Pfeiffer et al., 2010; Pfeiffer et al., 2012)
20XUAS-IVS-GCaMP6f (attP40)	Genetically-encoded calcium indicator	(Chen et al., 2013)

**Table of Genotypes**

Figure 1A	ChAT-Gal4.7.4/ pJFRC7-20XUAS-IVS-mCD8::GFP (attp40)
Figure 1C	R38b08-LexA (attp40)/+; pJFRC15-13XLexAop2-mCD8::GFP (attp2)/+ R48a07-LexA (attp40)/+; pJFRC15-13XLexAop2-mCD8::GFP (attp2)/+ 0203-LexA/pJFRC15-13XLexAop2-mCD8::GFP (attp2) iav-LexA(VK00013)/pJFRC15-13XLexAop2-mCD8::GFP (attp2)
Figure 2A	R38b08-LexA (attp40)/+; 13XLexAop2-IVS-Syn21-Chrimson::tdT-3.1-p10-F8 (VK00005)/+
Figure 2C-G	R38b08-LexA (attp40)/20XUAS-IVS-GCaMP6f (attP40); R57c10(nSyb)-Gal4 (attp2)/ 13XLexAop2-IVS-Syn21-Chrimson::tdT-3.1-p10-F8 (VK00005)
Figure 3	pJFRC7-20XUAS-IVS-mCD8::GFP (attp40);R13d11-Gal4 (attp2) pJFRC7-20XUAS-IVS-mCD8::GFP (attp40);R69c05-Gal4 (attp2) pJFRC7-20XUAS-IVS-mCD8::GFP (attp40);R18g08-Gal4 (attp2)
Figure 4A-B	R38b08-LexA (attp40)/ 13XLexAop2-IVS-Syn21-Chrimson::tdT-3.1-p10-F8 (su(Hw)attP5); R13d11-Gal4 (attp2)/ pJFRC7-20XUAS-IVS-mCD8::GFP (attp2)
Figure 4D-E	pJFRC7-20XUAS-IVS-mCD8::GFP (attp40)/ 13XLexAop2-IVS-Syn21-Chrimson::tdT-3.1-p10-F8 (su(Hw)attP5);R13d11-Gal4 (attp2)/ iav-LexA (VK00013)
Figure 5	R38b08-LexA (attp40)/ 13XLexAop2-IVS-Syn21-Chrimson::tdT-3.1-p10-F8 (su(Hw)attP5); R69c05-Gal4 (attp2)/ pJFRC7-20XUAS-IVS-mCD8::GFP (attp2)
Figure 6	R38b08-LexA (attp40)/ 13XLexAop2-IVS-Syn21-Chrimson::tdT-3.1-p10-F8 (su(Hw)attP5); R18g08-Gal4 (attp2)/ pJFRC7-20XUAS-IVS-mCD8::GFP (attp2)
Figure 7	pJFRC7-20XUAS-IVS-mCD8::GFP; R13d11-Gal4/R18g08-Gal4 pJFRC7-20XUAS-IVS-mCD8::GFP; R13d11-Gal4/R69c05-Gal4
Figure S1	R38b08-LexA (attp40)/+; pJFRC15-13XLexAop2-mCD8::GFP (attp2)/+ R48a07-LexA (attp40)/+; pJFRC15-13XLexAop2-mCD8::GFP (attp2)/+ 0203-LexA/pJFRC15-13XLexAop2-mCD8::GFP (attp2) iav-LexA(VK00013)/pJFRC15-13XLexAop2-mCD8::GFP (attp2)
Figure S2	R38b08-LexA (attp40)/+; pJFRC15-13XLexAop2-mCD8::GFP (attp2)/+ R48a07-LexA (attp40)/+; pJFRC15-13XLexAop2-mCD8::GFP (attp2)/+ 0203-LexA/pJFRC15-13XLexAop2-mCD8::GFP (attp2) iav-LexA(VK00013)/pJFRC15-13XLexAop2-mCD8::GFP (attp2)
Figure S3	pJFRC7-20XUAS-IVS-mCD8::GFP (attp40);R13d11-Gal4 (attp2) pJFRC7-20XUAS-IVS-mCD8::GFP (attp40);R69c05-Gal4 (attp2)

	pJFRC7-20XUAS-IVS-mCD8::GFP (attp40);R18g08-Gal4 (attp2)
Figure S4	pJFRC7-20XUAS-IVS-mCD8::GFP (attp40);R13d11-Gal4 (attp2) pJFRC7-20XUAS-IVS-mCD8::GFP (attp40);R69c05-Gal4 (attp2) pJFRC7-20XUAS-IVS-mCD8::GFP (attp40);R18g08-Gal4 (attp2)
Figure S5	pJFRC7-20XUAS-IVS-mCD8::GFP (attp40);R13d11-Gal4 (attp2) pJFRC7-20XUAS-IVS-mCD8::GFP (attp40);R69c05-Gal4 (attp2) pJFRC7-20XUAS-IVS-mCD8::GFP (attp40);R18g08-Gal4 (attp2)
Figure S6	pJFRC7-20XUAS-IVS-mCD8::GFP (attp40);R13d11-Gal4 (attp2) pJFRC7-20XUAS-IVS-mCD8::GFP (attp40);R69c05-Gal4 (attp2) pJFRC7-20XUAS-IVS-mCD8::GFP (attp40);R18g08-Gal4 (attp2) 47c08-LexA (attp40)/ 13XLexAop2-IVS-Syn21-Chrimson::tdT-3.1-p10-F8 (su(Hw)attP5); R13d11-Gal4 (attp2)/ pJFRC7-20XUAS-IVS-mCD8::GFP (attp2)
Figure S7	R38b08-LexA (attp40)/ 13XLexAop2-IVS-Syn21-Chrimson::tdT-3.1-p10-F8 (su(Hw)attP5); R18g08-Gal4 (attp2)/ pJFRC7-20XUAS-IVS-mCD8::GFP (attp2)
Table S1	R48a07-LexA (attp40)/ 13XLexAop2-IVS-Syn21-Chrimson::tdT-3.1-p10-F8 (su(Hw)attP5); R13d11-Gal4 (attp2)/ pJFRC7-20XUAS-IVS-mCD8::GFP (attp2) R48a07-LexA (attp40)/ 13XLexAop2-IVS-Syn21-Chrimson::tdT-3.1-p10-F8 (su(Hw)attP5); R69c05-Gal4 (attp2)/ pJFRC7-20XUAS-IVS-mCD8::GFP (attp2) R48a07-LexA (attp40)/ 13XLexAop2-IVS-Syn21-Chrimson::tdT-3.1-p10-F8 (su(Hw)attP5); R18g08-Gal4 (attp2)/ pJFRC7-20XUAS-IVS-mCD8::GFP (attp2) pJFRC7-20XUAS-IVS-mCD8::GFP (attp40)/ 13XLexAop2-IVS-Syn21-Chrimson::tdT-3.1-p10- F8 (su(Hw)attP5);R18g08-Gal4 (attp2)/ iav-LexA (VK00013) pJFRC7-20XUAS-IVS-mCD8::GFP (attp40)/ 13XLexAop2-IVS-Syn21-Chrimson::tdT-3.1-p10- F8 (su(Hw)attP5);R69c05-Gal4 (attp2)/ iav-LexA (VK00013) pJFRC7-20XUAS-IVS-mCD8::GFP (attp40)/ 13XLexAop2-IVS-Syn21-Chrimson::tdT-3.1-p10- F8 (su(Hw)attP5);R13d11-Gal4 (attp2)/ 0203-LexA pJFRC7-20XUAS-IVS-mCD8::GFP (attp40)/ 13XLexAop2-IVS-Syn21-Chrimson::tdT-3.1-p10- F8 (su(Hw)attP5);R18g08-Gal4 (attp2)/ 0203-LexA pJFRC7-20XUAS-IVS-mCD8::GFP (attp40)/ 13XLexAop2-IVS-Syn21-Chrimson::tdT-3.1-p10- F8 (su(Hw)attP5);R69c05-Gal4 (attp2)/ 0203-LexA

**Table S1**

	<b>R13d11-GAL4 (intersegmental)</b>	<b>R69c05-GAL4 (local)</b>	<b>R18g08-GAL4 (projection)</b>	<b>Motor neurons (control)</b>
<b>R38b08-LexA (bristles)</b>	excitation: entire ipsilateral leg (n > 10), blocked by 1 $\mu$ M MLA	excitation: distal ipsilateral leg (n > 10), blocked by 1 $\mu$ M MLA  inhibition: proximal ipsilateral leg (n > 10) blocked by 10 $\mu$ M picrotoxin	excitaiton: ipsilateral and contralateral legs (n > 10), blocked by 1 $\mu$ M MLA  inhibition: ipsilateral and contralateral legs (n > 10), blocked by 10 $\mu$ M picrotoxin	
<b>iav-LexA (chordotonal)</b>	inhibition: prothoracic ipsilateral femur (n=9), blocked by 100 $\mu$ M picrotoxin and 50 $\mu$ M CGP54626	no response to peripheral light stimuli on ipsilateral leg (n=2)	no response to peripheral light stimuli on ipsilateral leg (n=3)	excitation: prothoracic ipsilateral femur (n=2)
<b>R48a07-LexA (hair plates)</b>	no response to peripheral light stimuli on ipsilateral leg (n=2)	no response to peripheral light stimuli on ipsilateral leg (n=2)	no response to peripheral light stimuli on ipsilateral leg (n=2)	excitation: prothoracic ipsilateral femur (n=2), blocked by 1 $\mu$ M TTX in 1 prep
<b>0203-LexA (campaniform)</b>	no response to peripheral light stimuli on ipsilateral leg (n=2)	no response to peripheral light stimuli on ipsilateral leg (n=2)	no response to peripheral light stimuli on ipsilateral leg (n=2)	excitation: prothoracic ipsilateral femur (n = 5), blocked by 1 $\mu$ M MLA in 2 preps

**Table S1, related to Figures 4-6. Table of mechanoreceptor/central neuron connectivity**

This table provides a summary of all the pairwise combinations of mechanoreceptor and central neurons we tested for functional connectivity. For each combination, Chrimson was driven in peripheral mechanoreceptors under the control of LexA (rows), while central neurons were labeled with mCD8::GFP under the control of GAL4 (columns). Whole-cell recordings were targeted to central neurons, and a spot on the leg was stimulated with light through an optical fiber (see Methods for details). The spot was moved during the experiment so that the entire leg was ultimately illuminated. For cases in which we did not observe a postsynaptic response, we confirmed that optogenetic stimulation was working by recording light-evoked activity from unlabeled motor neurons, which were identified based on their large, lateral cell bodies. Thus, we are confident that these negative results are not due to inefficacy of our optogenetic methods, but rather due to lack of connectivity.

## References

- Buchner, E., Buchner, S., Burg, M.G., Hofbauer, A., Pak, W.L., and Pollack, I. (1993). Histamine is a major mechanosensory neurotransmitter candidate in *Drosophila melanogaster*. *Cell Tissue Res.* 273, 119-125.
- Burrows, M. (1996). *Neurobiology of an Insect Brain* (Oxford: Oxford University Press).
- Chen, T.W., Wardill, T.J., Sun, Y., Pulver, S.R., Renninger, S.L., Baohan, A., Schreiter, E.R., Kerr, R.A., Orger, M.B., Jayaraman, V., *et al.* (2013). Ultrasensitive fluorescent proteins for imaging neuronal activity. *Nature* 499, 295-300.
- Corfas, G., and Dudai, Y. (1990). Adaptation and fatigue of a mechanosensory neuron in wild-type *Drosophila* and in memory mutants. *J. Neurosci.* 10, 491-499.
- Daniels, R.W., Gelfand, M.V., Collins, C.A., and DiAntonio, A. (2008). Visualizing glutamatergic cell bodies and synapses in *Drosophila* larval and adult CNS. *J. Comp. Neurol.* 508, 131-152.
- Gohl, D.M., Silies, M.A., Gao, X.J., Bhalerao, S., Luongo, F.J., Lin, C.C., Potter, C.J., and Clandinin, T.R. (2011). A versatile *in vivo* system for directed dissection of gene expression patterns. *Nat. Methods* 8, 231-237.
- Gouwens, N.W., and Wilson, R.I. (2009). Signal propagation in *Drosophila* central neurons. *J. Neurosci.* 29, 6239-6249.
- Grunert, U., and Gnatzy, W. (1987). K<sup>+</sup> and Ca<sup>++</sup> in the receptor lymph of arthropod cuticular mechanoreceptors. *J. Comp. Physiol. A* 161, 329-333.
- Guizar-Sicairos, M., Thurman, S.T., and Fienup, J.R. (2008). Efficient subpixel image registration algorithms. *Opt. Lett.* 33, 156-158.
- Hannah-Alava, A. (1958). Morphology and chaetotaxy of the legs of *Drosophila melanogaster*. *J. Morph.* 103, 281-310.
- Jenett, A., Rubin, Gerald M., Ngo, T.-T.B., Shepherd, D., Murphy, C., Dionne, H., Pfeiffer, Barret D., Cavallaro, A., Hall, D., Jeter, J., *et al.* (2012). A GAL4-Driver Line Resource for *Drosophila* Neurobiology. *Cell Rep.* 2, 991-1001.
- Kays, I., Cvetkovska, V., and Chen, B.E. (2014). Structural and functional analysis of single neurons to correlate synaptic connectivity with grooming behavior. *Nat. Protoc.* 9, 1-10.
- Kernan, M., Cowan, D., and Zuker, C. (1994). Genetic dissection of mechanosensory transduction: mechanoreception-defective mutations of *Drosophila*. *Neuron* 12, 1195-1206.
- Klapoetke, N.C., Murata, Y., Kim, S.S., Pulver, S.R., Birdsey-Benson, A., Cho, Y.K., Morimoto, T.K., Chuong, A.S., Carpenter, E.J., Tian, Z., *et al.* (2014). Independent optical excitation of distinct neural populations. *Nat. Methods* 11, 338-346.
- Liu, W.W., and Wilson, R.I. (2013). Glutamate is an inhibitory neurotransmitter in the *Drosophila* olfactory system. *Proc. Natl. Acad. Sci. USA* 110, 10294-10299.
- Melzig, J., Buchner, S., Wiebel, F., Wolf, R., Burg, M., Pak, W.L., and Buchner, E. (1996). Genetic depletion of histamine from the nervous system of *Drosophila* eliminates specific visual and mechanosensory behavior. *J. Comp. Physiol. A* 179, 763-773.
- Melzig, J., Burg, M., Gruhn, M., Pak, W.L., and Buchner, E. (1998). Selective histamine uptake rescues photo- and mechanoreceptor function of histidine decarboxylase-deficient *Drosophila* mutant. *J. Neurosci.* 18, 7160-7166.
- Pfeiffer, B.D., Ngo, T.T., Hibbard, K.L., Murphy, C., Jenett, A., Truman, J.W., and Rubin, G.M. (2010). Refinement of tools for targeted gene expression in *Drosophila*. *Genetics* 186, 735-755.
- Pfeiffer, B.D., Truman, J.W., and Rubin, G.M. (2012). Using translational enhancers to increase transgene expression in *Drosophila*. *Proc. Natl. Acad. Sci. USA* 109, 6626-6631.
- Pologruto, T.A., Sabatini, B.L., and Svoboda, K. (2003). ScanImage: flexible software for operating laser scanning microscopes. *Biomed Eng. Online* 2, 13.
- Salvaterra, P.M., and Kitamoto, T. (2001). *Drosophila* cholinergic neurons and processes visualized with Gal4/UAS-GFP. *Brain Res Gene Expr. Patterns* 1, 73-82.
- Schindelin, J.; Arganda-Carreras, I. & Frise, E. *et al.* (2012). Fiji: an open-source platform for biological-image analysis. *Nat. Methods* 9, 676-682.
- Shearin, H.K., Dvarishkis, A.R., Kozeluh, C.D., and Stowers, R.S. (2013). Expansion of the gateway multisite recombination cloning toolkit. *PLoS One* 8, e77724.
- Takagawa, K., and Salvaterra, P. (1996). Analysis of choline acetyltransferase protein in temperature sensitive mutant flies using newly generated monoclonal antibody. *Neurosci. Res.* 24, 237-243.
- Thurm, U., and Koppers, J. (1980). Epithelial physiology of insect sensilla. In *Insect Biology in the Future*, M. Locke, and D. Smith, eds. (New York: Academic Press, Inc), pp. 735-763.
- Wilson, R.I., and Laurent, G. (2005). Role of GABAergic inhibition in shaping odor-evoked spatiotemporal patterns in the *Drosophila* antennal lobe. *J. Neurosci.* 25, 9069-9079.
- Wilson, R.I., Turner, G.C., and Laurent, G. (2004). Transformation of olfactory representations in the *Drosophila* antennal lobe. *Science* 303, 366-370.